

# Universal Theory of Light Scattering of Randomly Oriented Particles: A Fluctuational-Electrodynamics Approach for Modeling of Light Transport in Disordered Nanostructures

Francisco V. Ramirez-Cuevas<sup>1,2</sup>, Kargal L. Gurunatha<sup>1</sup>, Ivan P. Parkin<sup>3</sup>, and Ioannis Papakonstantinou<sup>1,\*</sup>

<sup>1</sup>*Photonic Innovations lab, Department of Electronic and Electrical Engineering, University College London, London, WC1E 7JE, United Kingdom*

<sup>2</sup>*Facultad de Ingeniería y Ciencias, Universidad Adolfo Ibáñez, Santiago, Chile*

<sup>3</sup>*Department of Chemistry, University College London, London, WC1H 0AJ, United Kingdom*

\**Corresponding Author: i.papakonstantinou@ucl.ac.uk*

November 4, 2022

## Abstract

Disordered nanostructures are commonly encountered in many nanophotonic systems, from colloid dispersions for sensing, to heterostructured photocatalysts. Randomness, however, imposes severe challenges for nanophotonics modeling, often constrained by the irregular geometry of the scatterers involved or the stochastic nature of the problem itself. In this article, we resolve this conundrum by presenting a universal theory of averaged light scattering of randomly oriented objects. Specifically, we derive formulas of *orientation-and-polarization-averaged* absorption cross section, scattering cross section and asymmetry parameter, for single or collection of objects of arbitrary shape, and that can be solved by any electromagnetic scattering method. These three parameters can be directly integrated into traditional unpolarized radiative energy transfer modelling, enabling a practical tool to predict multiple scattering and light transport in disordered nanostructured materials. Remarkably, the formulas of average light scattering can be derived under the principles of fluctuational electrodynamics, allowing analogous mathematical treatment to the methods used in thermal radiation, non-equilibrium electromagnetic forces, and other associated phenomena. The proposed modelling framework is validated against optical measurements of polymer composite films with metal-oxide microcrystals. Our work sets a new paradigm in the theory of light scattering, that may contribute to a better understanding of light-matter interactions in applications such as, plasmonics for sensing and photothermal therapy, photocatalysts for water splitting and CO<sub>2</sub> dissociation, photonic glasses for artificial structural colours, diffuse reflectors for radiative cooling, to name just a few.

## Introduction

Predicting the complex optical phenomena manifesting in disordered nanomaterials represents a major challenge in the field of computational modeling. Plasmonic nanoparticle dispersions for sensing and photothermal therapy,<sup>1,2</sup> heterostructured photocatalysts for water splitting and CO<sub>2</sub> dissociation,<sup>3</sup> diffuse reflectors for radiative cooling,<sup>4</sup> and porous membranes for solar water desalination,<sup>5</sup> are a few examples where the complex interrelation between near-field coupling and multi-scattering interactions with variation in particle morphology, orientation and size impose severe limitations to theoretically predict the system optical response. Conventional modeling based on computational electromagnetics, such as the Finite Difference or Finite Elements methods, are often unsuitable to quantify the macroscopic optical properties of random media — namely their specular and total transmittance/reflectance

or the intensity distribution—, all critical to assess the performance of these systems. Stochastic methods appear as the most appropriate alternative to calculate these properties, yet their applicability is limited to composite media containing subwavelength structures (effective media approximations),<sup>6</sup> or spherical particles (radiative transfer simulations).<sup>7</sup> As a result of the limitations in modeling, the majority of designs in disordered nanophotonic materials are driven by a phenomenological approach, whereby multiple samples are fabricated and tested in an iterative process that is time-consuming and expensive.

Light transport in random media is commonly addressed through the radiative transfer theory,<sup>8,9</sup> which describes the propagation of the light specific intensity through a composite medium containing a random distribution of independently scattering particles. It is notable that, in principle, the theory is applicable to arbitrary particle geometries and groups of particles.<sup>9</sup> In practice, however,

radiative transfer modeling is commonly applied to study light transport in composites with spherical particles.<sup>7,10</sup> This is due to the scattering properties of the spherical particles being independent of the direction and polarization of the incident light.<sup>11</sup> In this particular scenario, the solution of the radiative transfer equation (RTE) for unpolarized light requires three parameters: the particle’s absorption cross section,  $C_{\text{abs}}$ , the scattering cross section,  $C_{\text{sca}}$ , and the asymmetry parameter,  $\mu_{\text{sca}}$ .<sup>7,12</sup> The latter is an indicator of the scattering anisotropy and a key element to calculate the angular distribution of scattered fields.<sup>12</sup>

The scattering of non-spherical particles, on the other hand, varies with the incident angle and polarization, and the RTE usually becomes too complex to solve.<sup>9</sup> Under the independent scattering approximation, however, the correlation of the scattered field from different particles vanishes<sup>9</sup> and the scattering properties of an ensemble of randomly oriented particles can be approximated by the orientation averaged from a single particle [Fig.1(a)]. For unpolarized light, the RTE becomes scalar,<sup>13</sup> and the *orientation and polarization averaged*  $C_{\text{abs}}$ ,  $C_{\text{sca}}$  and  $\mu_{\text{sca}}$  parameter triad can be used for radiative transfer simulations of arbitrary particles, following the same methodology of spherical particles. The same principle could be applied to more complex scenarios; for instance, a medium containing denser particle distributions or even particle clusters. In this case, the averaging should be performed over a properly chosen collection of particles, for which the effects from short range correlations (due to collective interaction and interference of scattered fields) are prevalent [Fig.1(b)].<sup>14</sup> Similarly, heterogeneous systems with particles of different size and/or optical properties can also be studied.

The computation of orientation and polarization average scattering (average scattering, from now onward) is, however, non-trivial. Standard brute-force methods based on averaging over many plane wave simulations at different angles of incidence and polarizations, can be computationally expensive. Alternatively, a variety of solutions for direct computation of average scattering have been proposed. The technique, implemented in the context of the T-Matrix method<sup>15,16</sup> and the Discrete Dipole Approximation (DDA),<sup>17</sup> consist in deriving semi-analytical formulas based on spherical waves expansion basis, which are averaged over a solid angle. However, even when the T-Matrix method and DDA are fundamentally applicable to objects of arbitrary geometry,<sup>14,18</sup> the restrictive use of spherical waves basis for average scattering calculations imposes major constrains. As such, the T-Matrix method for average scattering has only been demonstrated for cylinders,<sup>15</sup> spheroids,<sup>15</sup> and clusters of spherical particles;<sup>16</sup> while in the case of DDA, the efficiency of the algorithm is significantly reduced, as the method requires a spherical wave expansion over every sub-element in the discretization.<sup>17</sup> Furthermore, because the aforementioned methods for average scattering are based on mathemati-

cal derivations specifically tailored to T-Matrix and DDA, their implementation into alternative numerical methods is not trivial.

In this article, we present a universal theory of average light scattering for randomly oriented scatterers (single or collections of objects) of arbitrary shape, and demonstrate a practical methodology for radiative transfer simulations in disordered nanostructures. The paper is divided into five sections, followed by the conclusions. i) In the first section, we derive the formulas for *polarization-and-orientation-averaged*  $C_{\text{abs}}$ ,  $C_{\text{sca}}$  and  $\mu_{\text{sca}}$  for arbitrary shaped scatterers. The formulas are independent of the wave basis and, therefore, can be implemented by any computational method of electromagnetic scattering, such as T-Matrix Method,<sup>9</sup> Boundary elements method (BEM),<sup>19</sup> or DDA.<sup>17</sup> Based on these results, we evaluate the accuracy limits of other expressions for average light scattering commonly used in the literature.<sup>20,21</sup> ii) In the next section, we demonstrate that the formulas of average light scattering can be derived through the principles of fluctuational electrodynamics, and, hence, can be computed with the mathematical methods used in studies of near-field thermal radiation,<sup>22–25</sup> Casimir forces<sup>25</sup> and vacuum friction.<sup>26,27</sup> In this context, we develop a computational application to numerically compute averaged light scattering,<sup>28</sup> which is based on the fluctuating-surface-current BEM.<sup>29,30</sup> iii) In the following section, we validate the theory and simulation code for average scattering simulations against other analytical solutions.<sup>31</sup> iv) Next, we discuss how the three average light scattering parameters can be applied for modeling of radiative transfer in disordered nanostructures. v) The accuracy of the modeling framework is demonstrated in the final section, showing excellent agreement with optical measurements of polyethylene (PE) film composites with monoclinic vanadium dioxide [VO<sub>2</sub>(M)] microcrystals.

## Results

### Theory of average light scattering of randomly oriented particles

As discussed previously, light scattering from a collection of independent scatterers of arbitrary morphology and randomly oriented in space (Fig. 1), is equivalent to the average light scattering over all orientations and light polarizations.<sup>13</sup> We particularly focus on the average absorption cross section,  $\langle C_{\text{abs}} \rangle$ , scattering cross section,  $\langle C_{\text{sca}} \rangle$ , and asymmetry parameter,  $\langle \mu_{\text{sca}} \rangle$ , where  $\langle \dots \rangle = \frac{1}{4\pi} \sum_P \int (\dots) d\Omega$ , the  $P$  index runs over the two orthogonal polarizations, and  $\Omega$  is the solid angle. The asymmetry parameter,  $\mu_{\text{sca}}$ , defines the degree of anisotropy of scattering relative to the direction of the incident light

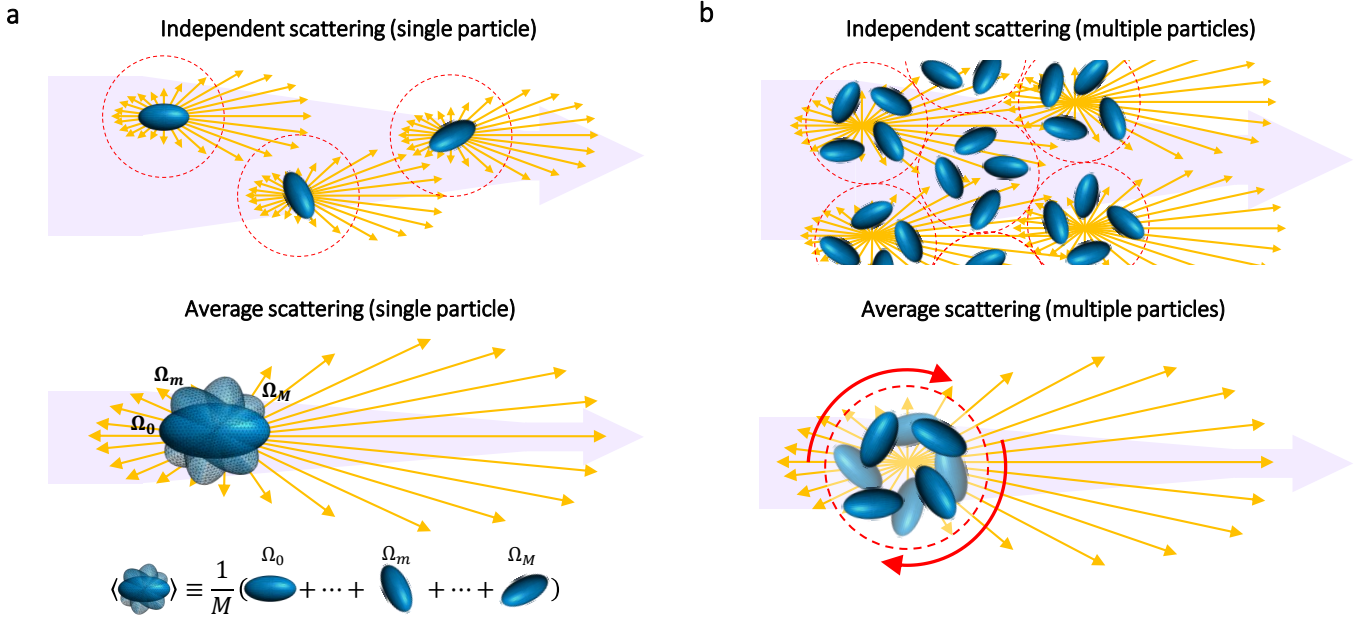


**Figure 1: Average scattering of randomly oriented particles.** (a) A collection of independent scattering particles (in this case prolate spheroids) randomly oriented in space, is approximated by the averaged sum over all possible particle's orientations (average scattering). In the bottom figure, the multiple orientations of the particle are labeled by  $\Omega_m$ , while  $M$  correspond to the total number of particle orientations considered in the averaging. In both schematics, the intensity of the incident light beam (purple arrow) decays due to scattering of the particle (yellow arrows). The red dotted circle represents a characteristic domain where short range correlations are relevant. (b) In more dense particle systems, the independent scattering approximation applies to a collection of particles within a properly chosen domain that consider the effects of short range correlations.<sup>14</sup> Average scattering, thus, is calculated over a characteristic collection of particles.

beam,  $\hat{\mathbf{k}}^i$ ,<sup>11</sup>

$$\mu_{\text{sca}} C_{\text{sca}} = \frac{1}{4\pi} \int_{4\pi} d\hat{\mathbf{k}}^s p_{\text{sca}}(\hat{\mathbf{k}}^s, \hat{\mathbf{k}}^i) \hat{\mathbf{k}}^s \cdot \hat{\mathbf{k}}^i,$$

where  $\hat{\mathbf{k}}^s$  is the direction of the scattered field and  $p_{\text{sca}}(\hat{\mathbf{k}}^s, \hat{\mathbf{k}}^i)$  is the scattering phase function.<sup>13</sup> By definition of  $p_{\text{sca}}$ ,  $C_{\text{sca}} = \frac{1}{4\pi} \int_{4\pi} d\hat{\mathbf{k}}^s p_{\text{sca}}(\hat{\mathbf{k}}^s, \hat{\mathbf{k}}^i)$ . Thus,  $\mu_{\text{sca}} > 0$  ( $\mu_{\text{sca}} < 0$ ), represent cases of forward (backward) anisotropic scattering and  $\mu_{\text{sca}} = 0$  represents isotropic scattering.

For our derivations, we consider the Lippmann-Schwinger approach, a general formalism to study electromagnetic scattering phenomena<sup>25</sup> In this approach, the scattered fields are given by,  $\mathbb{G}_0 \mathbb{T} \mathbf{E}^i$  [in this notation,  $\mathbb{T} \mathbf{E}^i = \int d^3 r' \mathbb{T}(\mathbf{r}, \mathbf{r}') \cdot \mathbf{E}^i(\mathbf{r}')$ ], where  $\mathbb{G}_0$  is the free space Dyadic Green function and  $\mathbb{T}$  is the scattering operator (Supporting Information, Eqs. (S4) and (S5), respectively). The mathematical form of the operators  $\mathbb{T}$  and  $\mathbb{G}_0$  is dictated by the expansion basis, and the geometry and optical properties of the scatterer. For example, for spherical wave basis applied on a spherical particle,  $\mathbb{T}(\mathbf{r}, \mathbf{r}') = \sum_l \int d^3 r'' \mathbf{f}_l^{\text{reg}}(\mathbf{r}) T_{ll} \mathbf{f}_l^{\text{reg}\dagger}(\mathbf{r}')$ , where  $\mathbf{f}_l^{\text{reg}}$  are spherical waves regular at the origin,  $T_{ll}$  are the Mie scattering coefficients, and  $\dagger$  is the conjugate transpose operator.<sup>25</sup> Likewise, in numerical methods for electromagnetic scattering, such as the T-Matrix Method,<sup>9</sup> BEM,<sup>19</sup> or DDA,<sup>17</sup> the mathematical form of  $\mathbb{T}$  and  $\mathbb{G}_0$  needs to

be determined prior to any scattering calculation.

Under the Lippmann-Schwinger approach, the formulas of  $C_{\text{abs}}$  and  $C_{\text{sca}}$  for an incident field  $\mathbf{E}^i$  are given by (details in Supporting Information, Section S1.1):<sup>24,32</sup>

$$C_{\text{abs}} = \frac{1}{k_0 |E_0|^2} \text{Tr} \left[ \left( \mathbf{E}^i \otimes \mathbf{E}^{i\dagger} \right) \mathbb{T}^\dagger \text{Asym}(-\mathbb{V}^{-1}) \mathbb{T} \right] \quad (1a)$$

$$C_{\text{sca}} = \frac{1}{k_0 |E_0|^2} \text{Tr} \left[ \left( \mathbf{E}^i \otimes \mathbf{E}^{i\dagger} \right) \mathbb{T}^\dagger \text{Asym}(\mathbb{G}_0) \mathbb{T} \right], \quad (1b)$$

where,  $k_0$  is the wavevector in free space and  $E_0$  is the amplitude of the incident fields;  $\mathbb{V}^{-1} = \mathbb{G}_0 - \mathbb{T}^{-1}$  is the particle's induced potential [Supporting Information, Eq. (S2)], and  $\otimes$  is the tensor product. The operators  $\text{Sym}(\mathbb{A}) = (\mathbb{A} + \mathbb{A}^\dagger)/2$  and  $\text{Asym}(\mathbb{A}) = (\mathbb{A} - \mathbb{A}^\dagger)/2i$ , represent the Hermitian and Anti-Hermitian part of  $\mathbb{A}$ , respectively. The trace is defined as  $\text{Tr}[\mathbb{A}] = \sum_l \int d^3 r \mathbb{A}_{ll}(\mathbf{r}, \mathbf{r})$ .

The formula of  $\mu_{\text{sca}}$  under the Lippmann-Schwinger approach, to the best of our knowledge, is presented here for the first time:

$$\mu_{\text{sca}} = -\frac{1}{k_0 |E_0|^2 C_{\text{sca}}} \sum_j \text{Tr} \left[ \hat{\mathbf{k}}_j^i \left( \mathbf{E}^i \otimes \mathbf{E}^{i\dagger} \right) \mathbb{T}^\dagger \text{Sym}(\partial_j \mathbb{G}_0) \mathbb{T} \right], \quad (1c)$$

where the index  $j$  in  $\hat{\mathbf{k}}_j^i$  and in the partial derivative  $\partial_j$ , represents the global coordinates of the system (*e.g.*,  $j =$

$x, y, z$ ). The formula is derived from the Lorentz force of the scattered fields over the induced currents in an object [Supporting Information, Eq. (S2)].

Because the operators  $\mathbb{T}$  and  $\mathbb{G}_0$  are dependent on the morphology and optical properties of the scatterer and not its orientation,  $\langle C_{\text{abs}} \rangle$  and  $\langle C_{\text{sca}} \rangle$  are uniquely determined by the expectation value of the incident fields,  $\langle \mathbf{E}^i \otimes \mathbf{E}^{i\dagger} \rangle$ , also known as the free space self-correlator.<sup>25</sup> Explicitly, this term is given by [see derivation in Supporting Information, Eq. (S10)]:

$$\langle \mathbf{E}^i \otimes \mathbf{E}^{i\dagger} \rangle = |E_0|^2 \frac{2\pi}{k_0} \text{Asym}(\mathbb{G}_0), \quad (2)$$

Similarly,  $\langle \mu_{\text{sca}} \rangle$  requires [see derivation in Supporting Information, Eq. (S11)]:

$$\langle \hat{\mathbf{k}}_j^i (\mathbf{E}^i \otimes \mathbf{E}^{i\dagger}) \rangle = -|E_0|^2 \frac{2\pi}{k_0} \text{Sym}(\partial_j \mathbb{G}_0). \quad (3)$$

Note that,  $\text{Asym}(\mathbb{G}_0) = \text{Im}(\mathbb{G}_0)$ , and  $\text{Sym}(\partial_j \mathbb{G}_0) = \partial_j \text{Im}(\mathbb{G}_0)$ , which stems from the properties of  $\mathbb{G}_0$  (reciprocal and symmetric dyadic) and  $\partial_j \mathbb{G}_0$  (reciprocal and anti-symmetric dyadic).<sup>33</sup>

The self-correlators in Eqs. (2) and (3) are the key elements for average scattering calculations. They enable simple and universal relations in terms of the dissipation in the free space [represented by  $\text{Im}(\mathbb{G}_0)$ ], alike to the expressions obtained from the fluctuation-dissipation theorem.<sup>23–25</sup> Using the self-correlators, we derive the following expressions:

$$\langle C_{\text{abs}} \rangle = \frac{2\pi}{k_0^2} \text{Tr} [\text{Asym}(\mathbb{G}_0) \mathbb{T}^\dagger \text{Asym}(-\mathbb{V}^{-1}) \mathbb{T}], \quad (4a)$$

$$\langle C_{\text{sca}} \rangle = \frac{2\pi}{k_0^2} \text{Tr} [\text{Asym}(\mathbb{G}_0) \mathbb{T}^\dagger \text{Asym}(\mathbb{G}_0) \mathbb{T}], \quad (4b)$$

$$\langle \mu_{\text{sca}} \rangle = \frac{1}{\langle C_{\text{sca}} \rangle} \frac{2\pi}{k_0^4} \sum_j \text{Tr} [\text{Sym}(\partial_j \mathbb{G}_0) \mathbb{T}^\dagger \text{Sym}(\partial_j \mathbb{G}_0) \mathbb{T}]. \quad (4c)$$

The three expressions represent universal recipe for average light scattering, compatible with any method for electromagnetic scattering (see an example for BEM in Supporting Information, Section S1.2). Moreover, because these relations are exclusively defined in terms of the operators  $\mathbb{T}$  and  $\mathbb{G}_0$ , they enable more efficient computation of  $\langle C_{\text{abs}} \rangle$ ,  $\langle C_{\text{sca}} \rangle$  and  $\langle \mu_{\text{sca}} \rangle$  than brute-force methods based on averaging over many plane wave simulations (see demonstration in Supporting Information, Section S1.2).

Eqs. (4a), (4b) and (4c) can be easily generalized for clustered particles and heterogeneous composites containing different types of particles (Supporting Information, Section S1.4). The light scattering parameters for an individual particle  $n$  in the cluster, i.e.,  $\langle C_{\text{abs}}^n \rangle$ ,  $\langle C_{\text{sca}}^n \rangle$  and  $\langle \mu_{\text{sca}}^n \rangle$ , are also obtained directly from these relations (details in Supporting Information, Section S1.5).

We finalize this section by discussing a common approximation for  $\langle C_{\text{abs}} \rangle$  found in the literature:<sup>20,21</sup>

$$\langle C_{\text{abs}} \rangle \approx \frac{1}{3} (C_{\text{abs},x} + C_{\text{abs},y} + C_{\text{abs},z}) \quad (5)$$

where  $C_{\text{abs},j}$  ( $j = x, y, z$ ) is the absorption cross section for an incident field polarized in the  $j$ -direction. As demonstrated in the Supporting Information (Section S1.6), Eq. (5) corresponds to a particular case of Eq. (4a) for small isolated objects. Similarly, we demonstrate that the analogous for scattering,<sup>20</sup> i.e.,  $\langle C_{\text{sca}} \rangle \approx \frac{1}{3} (C_{\text{sca},x} + C_{\text{sca},y} + C_{\text{sca},z})$  holds exact for spherical particles only (Supporting Information, Fig. S2).

### Average light scattering derived from fluctuational electrodynamics

The trace formulas for  $\langle C_{\text{abs}} \rangle$ ,  $\langle C_{\text{sca}} \rangle$  and  $\langle \mu_{\text{sca}} \rangle$  share many similarities with the relations found in studies of fluctuational electrodynamics, namely thermal radiation and non-equilibrium electromagnetic forces.<sup>25,29</sup> For example, in the framework of fluctuational electrodynamics, the thermal radiation absorbed by an isolated object,  $P_{\text{abs}}^{\text{th}}$ , is:<sup>25</sup>

$$P_{\text{abs}}^{\text{th}} = \int_0^\infty d\omega \Phi_{\text{abs}}(\omega) \Theta(\omega, T),$$

where  $\Phi_{\text{abs}}(\omega) = \frac{2}{\pi} \text{Tr} \{ \text{Asym}(\mathbb{G}_0) \mathbb{T}^\dagger \text{Asym}(-\mathbb{V}^{-1}) \mathbb{T} \}$ , and  $\Theta(\omega, T) = \frac{\hbar\omega}{\exp(\hbar\omega/k_B T) - 1}$ ;  $T$  is the temperature of the environment,  $\omega$  is the angular frequency,  $k_B$  is the Boltzmann constant, and  $\hbar$  is the reduced Planck constant. On the other hand, from light scattering theory,<sup>11</sup>  $P_{\text{abs}}^{\text{th}} = \int_0^\infty d\omega 4\pi \langle C_{\text{abs}} \rangle B_\omega(T)$ , where  $B_\omega(T) = \frac{k_0^2}{4\pi^3} \frac{\hbar\omega}{\exp(\hbar\omega/k_B T) - 1}$  is the Planck distribution. This leads to the relation:

$$\langle C_{\text{abs}} \rangle = \frac{\pi^2}{k_0^2} \Phi_{\text{abs}}(\omega). \quad (6)$$

This formula can be easily adapted to compute  $\langle C_{\text{sca}} \rangle$ , by replacing  $-\mathbb{V}^{-1}$  for  $\mathbb{G}_0$ .

Another relation comes from the electromagnetic friction induced by a moving photon gas on a stationary object.<sup>26,27</sup> To a first order approximation, the friction coefficient  $\gamma_f$ , can be expressed in terms of  $\langle C_{\text{abs}} \rangle$ ,  $\langle C_{\text{sca}} \rangle$  and  $\langle \mu_{\text{sca}} \rangle$  as (Supporting Information, Section S2.1):

$$\gamma_f = \frac{\hbar^2 k_0^4}{\pi^2 k_B T} \int_0^\infty d\omega \frac{e^{\hbar\omega/k_B T}}{(e^{\hbar\omega/k_B T} - 1)^2} \langle C_{\text{pr}} \rangle \quad (7)$$

where  $\langle C_{\text{pr}} \rangle = \langle C_{\text{ext}} \rangle - \langle \mu_{\text{sca}} C_{\text{sca}} \rangle$  and  $\langle C_{\text{ext}} \rangle = \langle C_{\text{abs}} \rangle + \langle C_{\text{sca}} \rangle$ , are the average radiation pressure and extinction cross sections, respectively.<sup>11</sup>

As illustrated by Eqs. (6) and (7), the formulas of average scattering can be derived by the principles of fluctuational electrodynamics. Consequently, the vast library of analytical solutions<sup>25,26</sup> and numerical algorithms<sup>29,35</sup> developed in the context of non-equilibrium energy and

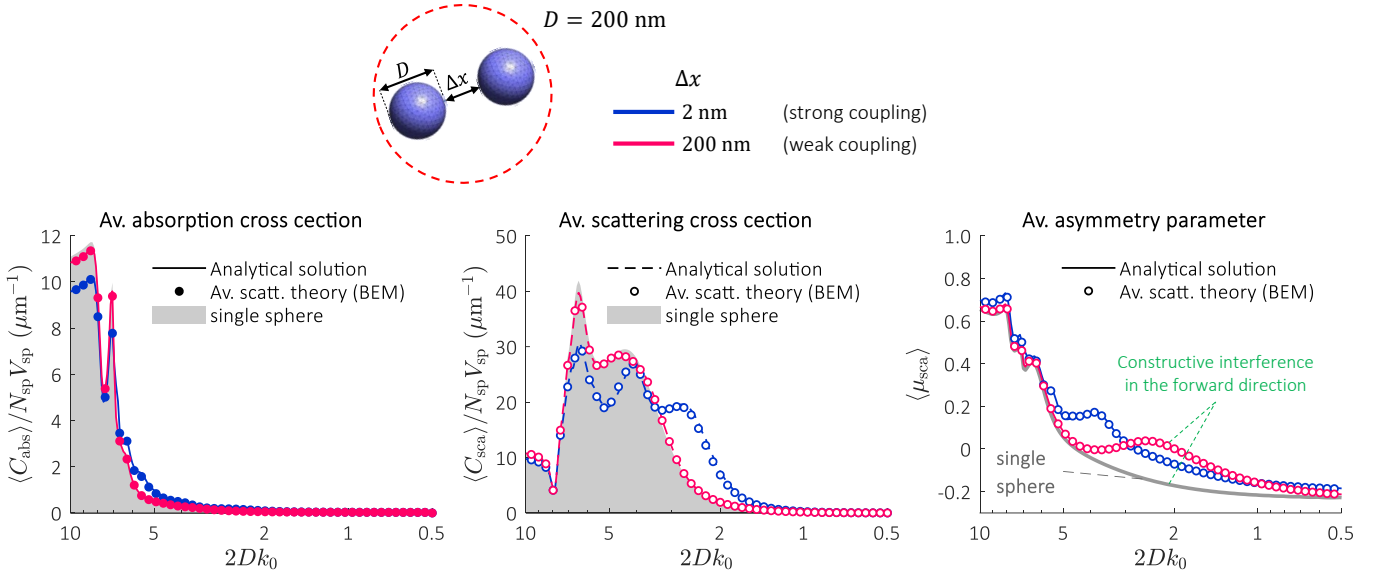


**Figure 2: Average light scattering of randomly oriented silver sphere dimer.**  $\langle C_{\text{abs}} \rangle$ ,  $\langle C_{\text{sca}} \rangle$  and  $\langle \mu_{\text{sca}} \rangle$  of the dimer as a function of the size parameter  $2Dk_0$  ( $k_0 = 2\pi/\lambda$ ). The curves  $\langle C_{\text{abs}} \rangle$  and  $\langle C_{\text{sca}} \rangle$  are normalized to the number of spheres,  $N_{\text{sp}} = 2$ , and spheres volume,  $V_{\text{sp}}$ , for direct comparison with the absorption and scattering cross section of a single sphere. The results are computed by the BEM code for average light scattering simulations,<sup>28</sup> and compared against the analytical solution.<sup>31</sup> The scattering parameters of a single sphere — i.e., absorption and scattering cross section normalized to the sphere’s volume (grey areas), and asymmetry parameter (grey curve) —, are computed from Mie-scattering<sup>11</sup> and plotted as a reference. The dielectric constant of silver can be found elsewhere.<sup>34</sup>

momentum transfer can be used to compute  $\langle C_{\text{abs}} \rangle$ ,  $\langle C_{\text{sca}} \rangle$  and  $\langle \mu_{\text{sca}} \rangle$ . For example, the thermal DDA<sup>35</sup> and fluctuating current BEM<sup>29</sup> for thermal radiation simulations, have explicit relations for  $\Phi_{\text{abs}}$  that can be adapted to compute  $\langle C_{\text{abs}} \rangle$  and  $\langle C_{\text{sca}} \rangle$ . On the other hand, the fluctuating current BEM also includes routines to compute  $\partial \mathcal{G}_0$ ,<sup>30</sup> which can be adapted for  $\langle \mu_{\text{sca}} \rangle$ .

In this context, we developed a computational code for average light scattering simulations, based on the fluctuating surface-current BEM formulation for non-equilibrium energy and momentum transfer.<sup>29,30</sup> The simulation code is implemented as an application of the SCUFF-EM software,<sup>36</sup> and can be accessed here.<sup>28</sup> Similar to other simulations tools based on BEM,<sup>29,30,37,38</sup> our code supports objects of arbitrary morphology and groups of objects (Supporting Information, Fig. S1), offering a convenient platform to explore the full potential of the average scattering theory presented here.

### Validation of average light scattering theory against analytical solutions

To validate the average scattering theory and BEM simulation code, we consider the problem of light scattering by a randomly oriented sphere dimer (Fig. 2), which has a known solution under the T-matrix approach.<sup>31</sup> The dimer consists of two silver spheres of diameter,  $D = 200$  nm, separated by a gap of i)  $\Delta x = 2$  nm and ii)  $\Delta x = 200$  nm. The results of a single sphere obtained from Mie

Scattering Theory,<sup>11</sup> are also plotted as a reference. Note that both the analytical solution and our theory of average light scattering are based on a classical approach, and, therefore, cannot capture quantum effects that may arise from these systems.

The results from the average scattering theory show excellent agreement with the analytical solution by Mishchenko et al.<sup>31</sup> (Fig. 2). When  $\Delta x = 2$  nm, the effects of electromagnetic coupling dominate and the average scattering curves of the dimer largely deviate from the response of a single sphere. When  $\Delta x = 200$  nm, the coupling effects weaken and both  $\langle C_{\text{abs}} \rangle$  and  $\langle C_{\text{sca}} \rangle$  approach to the response of a single sphere. However, this is not the case for  $\langle \mu_{\text{sca}} \rangle$ . Similar to the optical phenomenon observed in dilute particle media,<sup>41</sup> the scattered fields interfere constructively in the forward direction, which explains the discrepancy between the  $\langle \mu_{\text{sca}} \rangle$  curves.

As a second test, we consider the problems of average scattering from randomly oriented oblate and prolate spheroids, which has a known solution under the T-matrix approach.<sup>31</sup> The results are displayed in the Supporting Information (Fig. S3), showing excellent agreement up to  $L_{\text{max}}/\lambda \gtrsim 2.5$ , where  $L_{\text{max}}$  is the longest ellipsoid axis. At shorter wavelengths, there is a discrepancy of  $\sim 5\%$  associated to the size of the mesh used in BEM simulations. Even with this discrepancy, the results are consistent with the predictions from the analytical solution, allowing to validate the theory presented here.

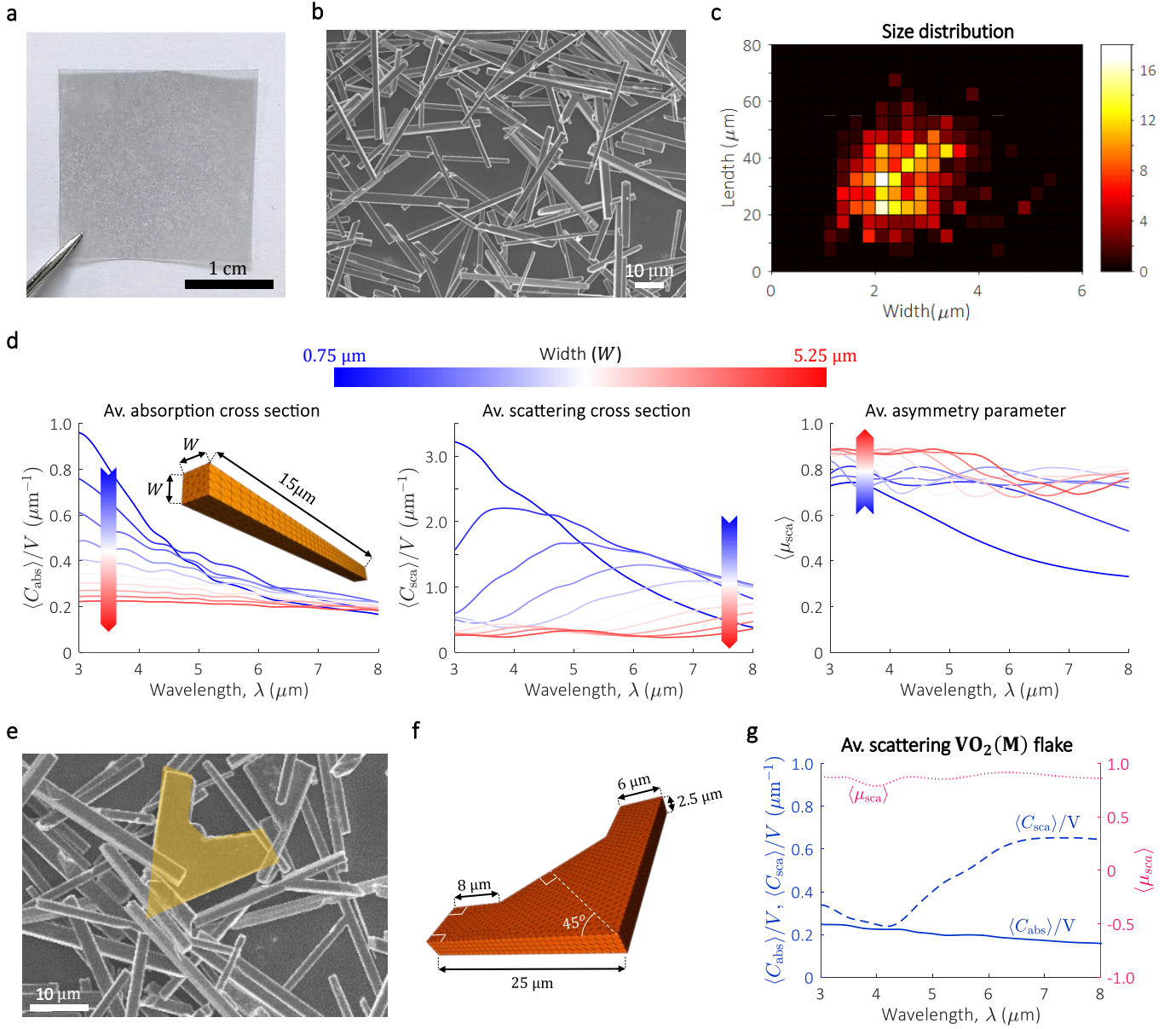


**Figure 3: Characterization and average scattering simulations of Monoclinic Vanadium Dioxide [VO<sub>2</sub>(M)] microcrystals embedded into a polyethylene (PE) matrix.** (a) Photograph of VO<sub>2</sub>(M)/PE composite film. (b) SEM of as-grown VO<sub>2</sub>(M) crystals, which is mainly composed of VO<sub>2</sub>(M) bars. (c) Size distribution of VO<sub>2</sub> bars. (d)  $\langle C_{\text{abs}} \rangle$ ,  $\langle C_{\text{sca}} \rangle$  and  $\langle \mu_{\text{sca}} \rangle$  of VO<sub>2</sub>(M) bars of fixed length,  $L = 15 \mu\text{m}$ , and variable width,  $W = 0.75 - 5.25 \mu\text{m}$  in steps of  $0.5 \mu\text{m}$ . The average scattering parameters showed similar dependence to  $W$  for other values of  $L$  (not shown here). The legend is given by the color bar at the top of the curves. (e) An example of one of the VO<sub>2</sub>(M) crystals with flake morphology found in the characteristic sample. (f) Computational representation of the VO<sub>2</sub>(M) flakes, which was considered for the average scattering simulations. (g) Simulated average light scattering of the VO<sub>2</sub>(M) flake. For all average scattering simulations, the refractive index of the host,  $n_{\text{host}} = 1.5$ , and the refractive index of the VO<sub>2</sub>(M) bars was obtained from the literature (see "film2" in Wan et al<sup>39</sup>).

### Radiative transfer modeling for random media with scatterers of arbitrary morphology

For unpolarized light and under the independent scattering approximation, the steady-state RTE for randomly ori-

ented scatterers in a non-absorbing host is:<sup>9</sup>

$$\hat{\mathbf{k}} \cdot \nabla_{\mathbf{r}} I_{\lambda}(\mathbf{r}, \hat{\mathbf{k}}) = -\frac{f_v}{V_p} \langle C_{\text{ext}} \rangle I_{\lambda}(\mathbf{r}, \hat{\mathbf{k}}) + \frac{f_v}{V_p} \int_{4\pi} d\hat{\mathbf{k}}' \langle p_{\text{sca}}(\cos \theta) \rangle I_{\lambda}(\mathbf{r}, \hat{\mathbf{k}}'), \quad (8)$$

where  $I_{\lambda}$  is the specific radiative intensity (defined as the energy flux per unit solid angle),  $f_v$  is the volume fraction,  $V_p$  is the effective volume of the scatterers,  $\hat{\mathbf{k}} \cdot \nabla_{\mathbf{r}} I_{\lambda}(\mathbf{r}, \hat{\mathbf{k}})$

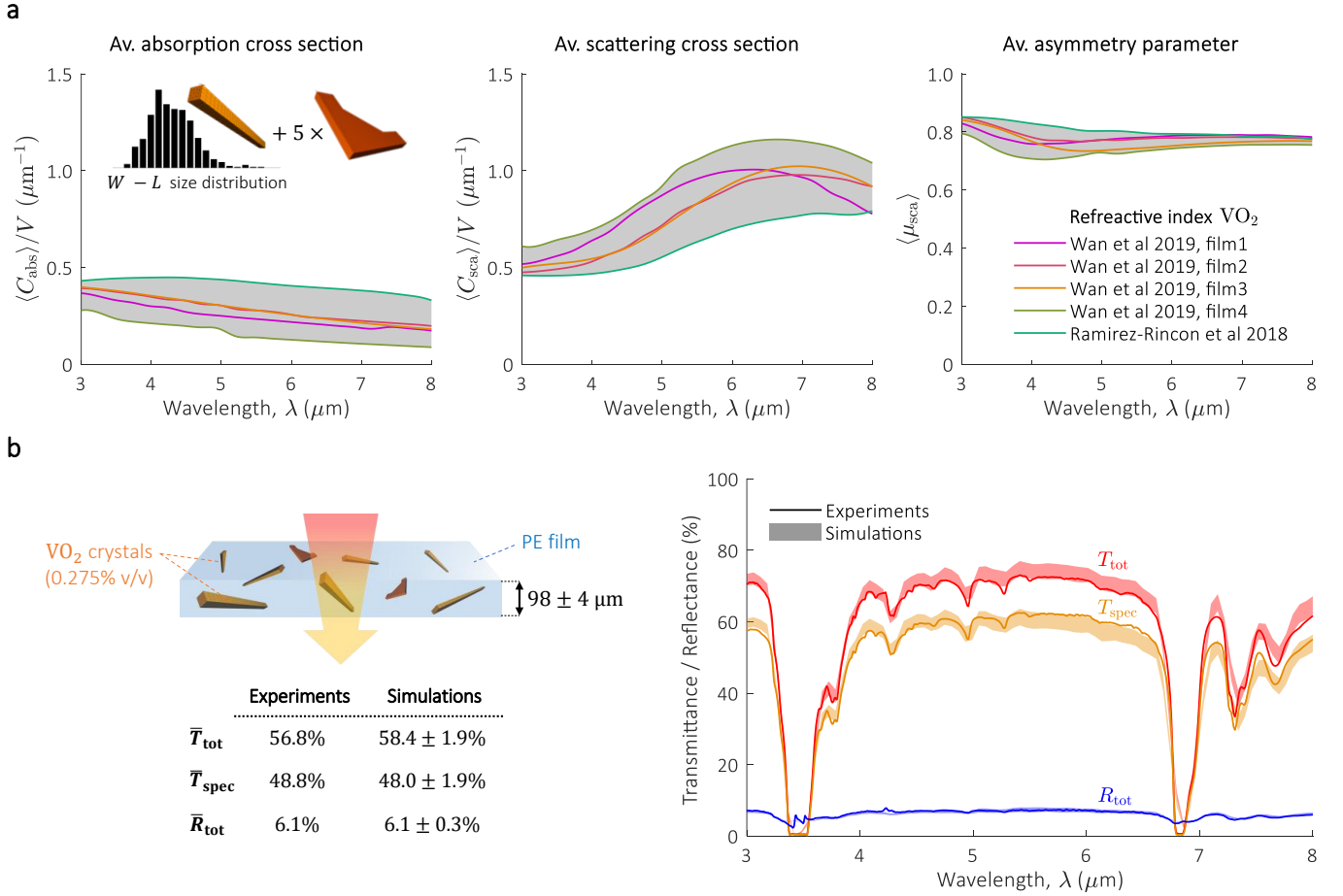


**Figure 4: Radiative transfer modeling of VO<sub>2</sub>(M)/PE film composite.** (a)  $\langle C_{\text{abs}} \rangle$ ,  $\langle C_{\text{sca}} \rangle$  and  $\langle \mu_{\text{sca}} \rangle$  of VO<sub>2</sub>(M) microcrystal ensemble calculated for five different refractive indexes of VO<sub>2</sub>(M), as reported by Wan et al 2019<sup>39</sup> (labeled as "film1", "film2", "film3" and "film4"), and Ramirez-Rincon et al 2018.<sup>40</sup> The grey areas mark the upper and lower limit due to variations in the refractive index. For a given refractive index, the curves  $\langle C_{\text{abs}} \rangle$ ,  $\langle C_{\text{sca}} \rangle$  and  $\langle \mu_{\text{sca}} \rangle$  were obtained as indicated by the schematic (left figure, inset), i.e. average scattering simulations of bars weighted by the size distribution + average scattering of 5 flakes. Further details in the Supporting Information, Section ???. The curves  $\langle C_{\text{abs}} \rangle$  and  $\langle C_{\text{sca}} \rangle$  are normalized to the volume of the ensemble  $V$  [Supporting Information, Eq. (??)]. (b) Validation of radiative transfer theory, showing  $T_{\text{tot}}$ ,  $T_{\text{spec}}$  and  $R_{\text{tot}}$  of a VO<sub>2</sub>(M)/PE composite film, as obtained from optical measurements (solid lines) and simulations (filled areas). The optical properties of the PE film were extracted from optical measurements on a clear film (see Supplement, Section ??). The composite is based on a 98 ± 4  $\mu\text{m}$  thick PE film with 0.275% v/v of VO<sub>2</sub>(M) microcrystals. The upper(lower) limit in the filled areas are the results of variations in the refractive index of VO<sub>2</sub>(M) and thickness of the film (98-4 or 98+4  $\mu\text{m}$ ).

is the rate of change of  $I_\lambda$  at the position,  $\mathbf{r}$ , and direction  $\hat{\mathbf{k}}$ ; and  $\langle p_{\text{sca}}(\cos\theta) \rangle$  is the orientation and polarization averaged scattering phase function, where  $\cos\theta = \hat{\mathbf{k}} \cdot \hat{\mathbf{k}}'$ . For simplicity, Eq. (8) omits the effects of emissivity that may arise, for example, due to luminescence or thermal emission.<sup>8,9,12</sup> However, their contribution can be easily included in the equation.<sup>12</sup> For example, the emitted thermal radiation from the scatterers can be represented by the adding the term  $\frac{f_p}{V_p} \langle C_{\text{abs}} \rangle B_\omega(T)$  to the right-hand side of the equation.<sup>12</sup> Similarly, if the host material is absorbing with an extinction coefficient,  $\kappa_{\text{host}}$ , its contribution must be included to the right-hand side of the equation, as:  $-2k_0\kappa_{\text{host}}I_\lambda(\mathbf{r}, \hat{\mathbf{k}})$ .

Commonly, solutions of Eq. (8) consider approximated expressions for the phase function in terms of  $\mu_{\text{sca}}$ .<sup>12</sup> For

example, the Henyey-Greenstein model:<sup>12</sup>

$$\langle p_{\text{sca}} \rangle = \langle C_{\text{sca}} \rangle \frac{1 - \langle \mu_{\text{sca}} \rangle^2}{[1 + \langle \mu_{\text{sca}} \rangle^2 - 2\langle \mu_{\text{sca}} \rangle \cos\theta]^{3/2}}, \quad (9)$$

is widely used in simulations methods, such as Monte-Carlo,<sup>7</sup> Adding-doubling<sup>42</sup> and Discrete Ordinate.<sup>12</sup>

As evidenced by Eqs. (8) and (9), the RTE and the average light scattering parameters  $\langle C_{\text{abs}} \rangle$ ,  $\langle C_{\text{sca}} \rangle$  and  $\langle \mu_{\text{sca}} \rangle$  constitute a complete set to model radiative transfer in composites with scatterers of arbitrary morphology. As demonstrated in the next section, this modeling framework enables to quantitatively predict the macroscopic radiative properties of a composite, such as the total transmittance ( $T_{\text{tot}}$ ), specular transmittance ( $T_{\text{spec}}$ ), and total reflectance ( $R_{\text{tot}}$ ).

## Validation of radiative transport simulation against experiments

We demonstrate the accuracy of the previously discussed modeling framework, by comparing the radiative transfer simulations against optical measurements of a composite based on VO<sub>2</sub>(M) microcrystals embedded in a polyethylene (PE) matrix [Fig. 3(a)]. We considered VO<sub>2</sub>(M) microcrystals given its well-defined and highly anisotropic morphology [Fig. 3(b)], providing an ideal scenario to validate the theory of average scattering and radiative transfer modeling. Additionally, the refractive index<sup>39,40</sup> and size of microcrystals, ensures a significant contribution from both absorption and scattering in the mid infrared (IR) spectrum.<sup>11</sup>

First, we derived the average light scattering parameters of the VO<sub>2</sub>(M) microcrystals ensemble using a characteristic sample Supporting Information, Fig. S4(c)]. The size distribution of the bars length ( $L$ ) and width ( $W$ ) is shown in Fig. 3(c), which assumes bars of square cross section. We calculated  $\langle C_{\text{abs}} \rangle$ ,  $\langle C_{\text{sca}} \rangle$  and  $\langle \mu_{\text{sca}} \rangle$  of single VO<sub>2</sub>(M) bars for  $\lambda = 3 - 8 \mu\text{m}$ , considering the range of  $W$  and  $L$  dictated by the size distribution. The spectrum  $\lambda > 8 \mu\text{m}$  is excluded in the simulations due to the large uncertainty in the refractive index of VO<sub>2</sub>(M), which is strongly conditioned by crystal orientation, growth method, strain and partial oxidation.<sup>39</sup> As shown in Fig. 3(d),  $\langle C_{\text{abs}} \rangle$ ,  $\langle C_{\text{sca}} \rangle$  and  $\langle \mu_{\text{sca}} \rangle$  are strongly sensitive to  $W$ . On the other hand, the three parameters are less sensitive to changes in  $L$ , with negligible variations for  $L > 15 \mu\text{m}$  (Supporting Information, Fig. S5). Additionally, the sample showed small traces of VO<sub>2</sub>(M) crystals of flake morphology, such as the one shown in Fig. 3(e). These VO<sub>2</sub>(M) flakes are represented by the computational model in Fig. 3(f), with the simulated average scattering parameters shown in Fig. 3(g).

The parameters  $\langle C_{\text{abs}} \rangle$ ,  $\langle C_{\text{sca}} \rangle$  and  $\langle \mu_{\text{sca}} \rangle$  of the VO<sub>2</sub>(M) microcrystals ensemble [Fig. 4(a)], were estimated using the average scattering simulations of individual bars and the flake, together with the size distribution. We repeated this procedure using five different refractive indexes reported in the literature,<sup>39,40</sup> in order to account for variations in the optical properties of VO<sub>2</sub>(M). The  $\langle C_{\text{abs}} \rangle$ ,  $\langle C_{\text{sca}} \rangle$  and  $\langle \mu_{\text{sca}} \rangle$  of the VO<sub>2</sub>(M) microcrystals ensemble together with radiative transfer simulations [Eq. (8)], are used to estimate  $T_{\text{tot}}$ ,  $T_{\text{spec}}$  and  $R_{\text{tot}}$  of a VO<sub>2</sub>(M)/PE composite film [Fig. 4(b)]. Radiative transfer simulations are performed by the Monte-Carlo method (see details in Methods). The results are shown by filled areas, representing the upper and lower limits associated with the variations of the refractive index of VO<sub>2</sub>(M) and thickness of the film. The experimental optical measurements show excellent agreement with the range predicted by simulations, which is further confirmed by the spectral mean of  $T_{\text{tot}}$ ,  $T_{\text{spec}}$  and  $R_{\text{tot}}$  [Table in Fig. 4(b)]. The accuracy of the simulation is further confirmed through a second test,

which considers a composite film with double concentration of VO<sub>2</sub>(M) microcrystals (Supporting Information, Fig. S7).

## Conclusion

In this paper, we presented a universal theory to predict the average light scattering from randomly oriented objects with arbitrary shape. The formulas of  $\langle C_{\text{abs}} \rangle$ ,  $\langle C_{\text{sca}} \rangle$  and  $\langle \mu_{\text{sca}} \rangle$  represent a recipe for efficient computation of average light scattering, that can be implemented by any method of electromagnetic scattering. The abstract format of these formulas provides a convenient landscape to explore the fundamental limits of scattering in random systems, as demonstrated in other studies of bounds in scattering and absorption.<sup>24,32</sup> In this context, for example, the formula of asymmetry parameter [Eq. (4c)] can be used to evaluate the limits for maximum forward or backward scattering under a set of particular constrains. On the other hand, the demonstrated connection between average light scattering and fluctuational electrodynamics, enables to extend the theory to other parameters of interest in the field of light-matter interactions in disordered nanostructures. For example, a formula for the average scattering of moving objects can be extracted from the theory of electromagnetic friction induced by objects in relative motion.<sup>26</sup>

The parameters  $\langle C_{\text{abs}} \rangle$ ,  $\langle C_{\text{sca}} \rangle$  and  $\langle \mu_{\text{sca}} \rangle$  are also practical for radiative transfer simulations for unpolarized light, enabling accurate prediction of the radiative properties in composites with scatterers of arbitrary shape, as demonstrated in the study of VO<sub>2</sub>(M)/PE composite films. The methodology of this study can be applied to other composite media, with either dielectrics or metal scatterers, providing that the distance between particles is large enough to ignore the effects of short range correlations. For more complex problems, such as clustered particles or more dense particle distributions, our methodology can be extended using the formulation for multiple objects (Supporting Information, Section S1.4). In this case,  $\langle C_{\text{abs}} \rangle$ ,  $\langle C_{\text{sca}} \rangle$  and  $\langle \mu_{\text{sca}} \rangle$  must be obtained from simulations over a properly chosen collection of particles. The method, thus, could provide key insights to many problems in disordered nanophotonics, such as the effects of agglomeration into the optical absorption of gold nanostars, or the impact of multiple scattering in the light trapping of heterostructured photocatalysts, as we will discuss in future works.

In summary, the theory of average light scattering for randomly oriented objects establishes the underlying basis for fundamental studies in disordered nanophotonics. The combination with radiative transport theory enables a powerful modeling method to predict the macroscale optical response in random systems, setting new pathways for design and optimization of nanophotonic devices based on composites, synthesized nanostructures on substrates or

particles in solution.

## Methods

### Fabrication and characterization of VO<sub>2</sub>(M) / PE composite films

The composite was fabricated by dry mixing of VO<sub>2</sub>(M) microcrystals with low-density PE (LDPE; 42607, Sigma Aldrich) and Ultra-high-molecular-weight PE (UHMWPE; 429015, Sigma Aldrich) at a weight ratio of VO<sub>2</sub>(M):LDPE:UHMWPE = 1:40:40. The mixture was then melt-pressed into a film at 200°C. The VO<sub>2</sub>(M) crystals were produced by hydrothermal synthesis using our previously developed procedure.<sup>43</sup> The phase of the crystals was confirmed by X-ray diffraction and Raman spectroscopy [Supporting Information, Fig. S4(a) and S4(b), respectively]. The volume fraction of the VO<sub>2</sub>(M) microcrystals was estimated from the weight ratio and the densities of VO<sub>2</sub>(M) (4.230 g/cm<sup>3</sup>),<sup>44</sup> LDPE (0.925 g/cm<sup>3</sup>) and UHMWPE (0.940 g/cm<sup>3</sup>). A micrometer was used to characterize the thickness of the film. The reported thickness corresponds to 5 measurements on different sections of the sample.

### Optical measurements

The total and specular transmittance, and total reflectance of the VO<sub>2</sub>(M)/polyethylene composite film were measured with a Fourier-transform-infrared spectrometer (IRTracer-100, Shimadzu) and a mid-IR Integrating sphere (Pike Technologies).

### Monte-Carlo simulations of radiative transfer

Radiative transfer simulations were performed by our own code for Monte-Carlo simulations of unpolarized light. The algorithm consist on simulating the trajectories of many individual photons as they interact with particles and interfaces, until they are either, absorbed by particles or exit the simulation domain. The initial condition of each photon is given by the position and direction of the light source. At each simulation step, the optical path ( $\Lambda_{\text{photon}}$ ) and fate of a photon is estimated by selecting the shortest path between the particle's scattering ( $\Lambda_{\text{sca}}$ ) and absorption ( $\Lambda_{\text{abs}}$ ), the absorption of the host ( $\Lambda_{\text{host}}$ ), or diffraction ( $\Lambda_{\text{Fresnel}}$ ), where:

$$\begin{aligned}\Lambda_{\text{sca}} &= -\frac{V_p}{f_v \langle C_{\text{sca}} \rangle} \ln \xi, \\ \Lambda_{\text{abs}} &= -\frac{V_p}{f_v \langle C_{\text{abs}} \rangle} \ln \xi, \\ \Lambda_{\text{host}} &= -2k_0 \kappa_{\text{host}} \ln \xi,\end{aligned}$$

and  $\xi$  is a random number between 0 and 1;  $\Lambda_{\text{Fresnel}}$  is given by the shortest distance between the photon and an interface. In materials with more than one kind of particle,  $\Lambda_{\text{abs}} = \min(\Lambda_{\text{abs}}^i)$  and  $\Lambda_{\text{sca}} = \min(\Lambda_{\text{sca}}^n)$ , where  $\Lambda_{\text{abs}}^i$  and  $\Lambda_{\text{sca}}^n$  are, respectively, the absorption and scattering path from the particle  $n$ .

In the case of diffraction ( $\Lambda_{\text{photon}} = \Lambda_{\text{Fresnel}}$ ), a photon is either reflected or transmitted by a random selection, with the probabilities of each event proportional to the respective energy flux defined by Fresnel laws. If the photon is absorbed by a particle ( $\Lambda_{\text{photon}} = \Lambda_{\text{abs}}$ ) or the host material ( $\Lambda_{\text{photon}} = \Lambda_{\text{host}}$ ), the event is terminated and the simulation continues with a new photon at the initial conditions. For a scattered photon ( $\Lambda_{\text{photon}} = \Lambda_{\text{sca}}$ ), the new direction is determined by:<sup>7</sup>

$$\cos \theta = \begin{cases} \frac{1}{2g} \left\{ 1 + g^2 - \left[ \frac{1-g^2}{1-g+2g\xi} \right]^2 \right\}, & \text{if } g \neq 0, \\ 2\xi - 1, & \text{if } g = 0, \end{cases}$$

where  $g = \langle \mu_{\text{sca}} \rangle$ .

In all our simulations, we considered a slab with large surface area, in order to represent a 2D problem. As a criteria, we selected the smallest surface area by which no photon escapes through the edges. Two large monitors, above and below the slab, measure the total reflectance and transmittance, respectively. The specular transmittance was measured with a third small monitor (1 nm × 1 nm) at 1 mm distance below the slab. In all the simulation, we considered 1,000,000 photons per wavelength. For validation of our code, refer to Supporting Information, Section S5.

## References

1. Langer, J. *et al.* “Present and future of surface-enhanced Raman scattering”. *ACS Nano* **14**, 28–117 (2020).
2. Cheng, L. *et al.* “Functional nanomaterials for phototherapies of cancer”. *Chemical Reviews* **114**, 10869–10939 (2014).
3. Low, J. *et al.* “Heterojunction Photocatalysts”. *Advanced Materials* **29**, 1601694 (May 2017).
4. Zhao, D. *et al.* “Radiative sky cooling: Fundamental principles, materials, and applications”. *Applied Physics Reviews* **6**, 021306 (2019).
5. Tao, P. *et al.* “Solar-driven interfacial evaporation”. *Nature Energy* **3**, 1031–1041 (Dec. 2018).
6. Cai, W. & Shalaev, V. *Optical Metamaterials: Fundamentals and Applications*, 200 (Springer, New York, USA, 2009).

7. Jacques, S. L. & Wang, L. “MCML—Monte Carlo modeling of light transport in multi-layered tissues”. *Computer Methods and Programs in Biomedicine* **47**, 131–146 (1995).
8. Ishimaru, A. *Wave Propagation and Scattering in Random Media* 1st, 600 (Oxford University Press, Oxford, UK, 1997).
9. Tsang, L. *et al.* *Scattering of Electromagnetic Waves: Theories and Applications*, 445 (John Wiley & Sons, Inc., New York, USA, 2000).
10. Hogan, N. J. *et al.* “Nanoparticles heat through light localization.” *Nano Letters* **14**, 4640–4645 (Aug. 2014).
11. Bohren, C. F. & Huffman, D. R. *Absorption and Scattering of Light by Small Particles*, 544 (John Wiley & Sons, Inc., 1998).
12. Stamnes, K., Thomas, G. E. & Stamnes, J. J. *Radiative Transfer in the Atmosphere and Ocean* 2nd, 531 (Cambridge University Press, Cambridge, UK, 2017).
13. Hulst, H. C. v. d. & Physics. *Light Scattering by Small Particles*, 470 (Dover Publications, Inc., New York, USA, 1981).
14. Tsang, L. *et al.* *Scattering of Electromagnetic Waves: Numerical Simulations*, 736 (John Wiley & Sons, Inc., 2001).
15. Bi, L. *et al.* “A numerical combination of extended boundary condition method and invariant imbedding method applied to light scattering by large spheroids and cylinders”. *Journal of Quantitative Spectroscopy and Radiative Transfer* **123**, 17–22 (2013).
16. Mackowski, D. W. & Mishchenko, M. I. “A multiple sphere T-matrix Fortran code for use on parallel computer clusters”. *Journal of Quantitative Spectroscopy and Radiative Transfer* **112**, 2182–2192 (2011).
17. Yurkin, M. A. & Hoekstra, A. G. “The discrete dipole approximation: An overview and recent developments”. *Journal of Quantitative Spectroscopy and Radiative Transfer* **106**, 558–589 (2007).
18. Mishchenko, M. I., Hovenier, J. W. & Travis, L. D. *Light scattering by nonspherical particles: theory, measurements, and applications* 1st, 720 (Academic Press, 2000).
19. Reid, M. T. & Johnson, S. G. “Efficient Computation of Power, Force, and Torque in BEM Scattering Calculations”. *IEEE Transactions on Antennas and Propagation* **63**, 3588–3598 (2015).
20. Santiago, E. Y. *et al.* “Efficiency of Hot-Electron Generation in Plasmonic Nanocrystals with Complex Shapes: Surface-Induced Scattering, Hot Spots, and Interband Transitions”. *ACS Photonics* **7**, 2807–2824 (2020).
21. Muskens, O. L. *et al.* “Quantitative absorption spectroscopy of a single gold nanorod”. *Journal of Physical Chemistry C* **112**, 8917–8921 (2008).
22. Liu, B., Li, J. & Shen, S. “Resonant Thermal Infrared Emitters in Near- and Far-Fields”. *ACS Photonics* **4**, 1552–1557 (2017).
23. Cuevas, J. C. & García-Vidal, F. J. “Radiative Heat Transfer”. *ACS Photonics* **5**, 3896–3915 (2018).
24. Molesky, S. *et al.* “T Operator Bounds on Angle-Integrated Absorption and Thermal Radiation for Arbitrary Objects”. *Physical Review Letters* **123**, 257401 (2019).
25. Krüger, M. *et al.* “Trace formulas for nonequilibrium Casimir interactions, heat radiation, and heat transfer for arbitrary objects”. *Physical Review B* **86**, 115423 (2012).
26. Golyk, V. A., Krüger, M. & Kardar, M. “Linear response relations in fluctuational electrodynamics”. *Physical Review B* **88**, 155117 (2013).
27. Mkrtchian, V. *et al.* “Universal thermal radiation drag on neutral objects”. *Physical Review Letters* **91**, 220801 (2003).
28. Ramirez-Cuevas, F. V. *AVESCATTER: A SCUFF-EM application for light scattering of randomly oriented particles of arbitrary shape*. 2020.
29. Rodriguez, A. W., Reid, M. T. & Johnson, S. G. “Fluctuating-surface-current formulation of radiative heat transfer: Theory and applications”. *Physical Review B* **88**, 054305 (Aug. 2013).
30. Reid, M. T. H. *et al.* “Photon Torpedoes and Rytov Pinwheels: Integral-Equation Modeling of Non-Equilibrium Fluctuation-Induced Forces and Torques on Nanoparticles”. *arXiv*, 18 (2017).
31. Mishchenko, M., Travis, L. & Mackowski, D. *T-Matrix Codes for Computing Electromagnetic Scattering by Nonspherical and Aggregated Particles*.
32. Molesky, S. *et al.* “Global T operator bounds on electromagnetic scattering: Upper bounds on far-field cross sections”. *Physical Review Research* **2**, 033172 (July 2020).
33. Tai, C.-T. *Dyadic Green Functions in Electromagnetic Theory* 2nd (ed Dudley, D. D.) 343 (IEEE Press Series, New York, USA, 1994).
34. Babar, S. & Weaver, J. H. “Optical constants of Cu, Ag, and Au revisited”. *Applied Optics* **54**, 477–481 (Jan. 2015).
35. Edalatpour, S. & Francoeur, M. “The Thermal Discrete Dipole Approximation (T-DDA) for near-field radiative heat transfer simulations in three-dimensional arbitrary geometries”. *Journal of Quantitative Spectroscopy and Radiative Transfer* **133**, 364–373 (2014).

36. Reid, M. T. H. *SCUFF-EM: Free, open-source software for boundary-element analysis of problems in computational physics and engineering*. 2014.
37. Solís, D. M. *et al.* “[Toward Ultimate Nanoplasmonics Modeling](#)”. *ACS Nano* **8**, 7559–7570 (Aug. 2014).
38. Solís, D. M. *et al.* “[Optimization of Nanoparticle-Based SERS Substrates through Large-Scale Realistic Simulations](#)”. *ACS Photonics* **4**, 329–337 (2017).
39. Wan, C. *et al.* “[On the Optical Properties of Thin-Film Vanadium Dioxide from the Visible to the Far Infrared](#)”. *Annalen der Physik* **531**, 1900188 (2019).
40. Ramirez-Rincon, J. A. *et al.* “[Thermal hysteresis measurement of the VO<sub>2</sub> dielectric function for its metal-insulator transition by visible-IR ellipsometry](#)”. *Journal of Applied Physics* **124**, 195102 (2018).
41. Hecht, E. *Optics* 5th, 714 (Pearson Education, Essex, UK, 2016).
42. Prah, S. A., van Gemert, M. J. C. & Welch, A. J. “[Determining the optical properties of turbid media by using the adding-doubling method](#)”. *Applied Optics* **32**, 559–568 (1993).
43. Gurunatha, K. L. *et al.* “[Combined Effect of Temperature Induced Strain and Oxygen Vacancy on Metal-Insulator Transition of VO<sub>2</sub> Colloidal Particles](#)”. *Advanced Functional Materials* **30**, 2005311 (2020).
44. Jain, A. *et al.* “[Commentary: The materials project: A materials genome approach to accelerating materials innovation](#)”. *APL Materials* **1**, 011002 (July 2013).

## Acknowledgements

The authors acknowledge the generous financial support from the H2020 European Research Council (ERC) starting grant IntelGlazing grant no: 679891.

## Author contributions statement

F.V.R and I.P designed the research. F.V.R developed the theory and simulation codes, performed the simulations, and carried the optical measurements. K.L.G carried synthesis and characterization of VO<sub>2</sub> (M) bars, and fabricated the VO<sub>2</sub>(M)/PE composite films. I.P and I.P.P facilitated the research. All authors contributed to writing and reviewing the paper.

## Additional information

The authors declare no competing interest

# Supporting Information for "Universal Theory of Light Scattering of Randomly Oriented Particles: A Fluctuational-Electrodynamics Approach for Modeling of Light Transport in Disordered Nanostructures"

Francisco V. Ramirez-Cuevas<sup>1,2</sup>, Kargal L. Gurunatha<sup>1</sup>, Ivan P. Parkin<sup>3</sup>, and Ioannis Papakonstantinou<sup>1,\*</sup>

<sup>1</sup>*Photonic Innovations Lab, Department of Electronic and Electrical Engineering, University College London, London, WC1E 7JE, United Kingdom*

<sup>2</sup>*Facultad de Ingeniería y Ciencias, Universidad Adolfo Ibáñez, Santiago, Chile*

<sup>3</sup>*Department of Chemistry, University College London, London, WC1H 0AJ, United Kingdom*

\**Corresponding Author: i.papakonstantinou@ucl.ac.uk*

November 4, 2022

## Contents

<b>S1 Theory of average light scattering from random oriented particles</b>	<b>2</b>
S1.1 Formulation for a single object . . . . .	2
S1.2 Surface-current BEM formulation . . . . .	4
S1.3 Efficiency of the theory against brute-force averaging methods. . . . .	5
S1.4 Formulation for multiple objects . . . . .	6
S1.5 Formulation for an individual objects in a cluster . . . . .	7
S1.6 Approximation for subwavelength particles . . . . .	7
<b>S2 Average light scattering from fluctuational electrodynamics</b>	<b>8</b>
S2.1 Vacuum friction and averaged light scattering . . . . .	8
<b>S3 Validation of average light scattering theory against analytical solutions</b>	<b>9</b>
S3.1 Average light scattering of randomly oriented spheroids . . . . .	9
<b>S4 Validation of radiative transfer simulation against experiments</b>	<b>10</b>
S4.1 Characterization of as-grown VO <sub>2</sub> (M) microcrystals . . . . .	10
S4.2 Average light scattering of VO <sub>2</sub> (M) bars as a function of $L$ . . . . .	11
S4.3 Estimation of average light scattering of VO <sub>2</sub> (M) microcrystal ensemble . . . . .	11

S4.4 Prediction of refractive index and scattering from PE films . . . . .	11
S4.5 Radiative properties of VO <sub>2</sub> (M)/PE composite films (Experiments and Simulations . . . . .	13

**S5 Validation of Monte-Carlo Code** **13**

# S1 Theory of average light scattering from random oriented particles

## S1.1 Formulation for a single object

In the context of Lippmann-Schwinger approach,<sup>1</sup> the presence of a object in an infinitely extended medium 0 induces a perturbation to the incident (source) electric fields,  $\mathbf{E}^i$ , that results in a scattered (induced) electric field,  $\mathbf{E}^s$ , in medium 0. For simplicity, we consider medium 0 as vacuum, with electrical permittivity,  $\epsilon_0$ , and magnetic permeability,  $\mu_0$ , while the object is characterized by linear electromagnetic properties, i.e., dielectric constant,  $\epsilon$ , and relative permeability  $\mu$ , which can be, in general, nonlocal complex tensors. The total electric field,  $\mathbf{E}^t$ , that results from the superposition of  $\mathbf{E}^i$  and  $\mathbf{E}^s$ , satisfies the following equation:<sup>1</sup>

$$[\mathbb{H}_0 - k_0^2 \mathbb{I} - \mathbb{V}] \mathbf{E}^t = 0, \tag{S1}$$

where  $k_0 = \omega \sqrt{\epsilon_0 \mu_0}$  is the wavevector in free space,  $\mathbb{I}$  is the identity operator,  $\mathbb{H}_0 = \nabla \times \nabla \times$ , and

$$\mathbb{V} = k_0^2 (\epsilon - \mathbb{I}) + \nabla \times (\mu^{-1} - \mathbb{I}) \nabla \times \tag{S2}$$

is the induced potential by the object, with  $\mathbb{V} = 0$  anywhere outside the object.

Solution of Eq. (S1) is given by:

$$\mathbf{E}^t = (\mathbb{I} + \mathbb{G}_0 \mathbb{T}) \mathbf{E}^i, \tag{S3}$$

where  $\mathbb{G}_0$  is the free space dyadic green function:<sup>2</sup>

$$\mathbb{G}_0(\mathbf{r}, \mathbf{r}') = \left[ \mathbb{I} + \frac{1}{k_0^2} \nabla \nabla \right] \frac{e^{ik_0 |\mathbf{r} - \mathbf{r}'|}}{4\pi |\mathbf{r} - \mathbf{r}'|}, \tag{S4}$$

which satisfies  $[\mathbb{H}_0 - \mathbb{I}] \mathbb{G}_0 = \delta(\mathbf{r} - \mathbf{r}')$ , and  $\mathbb{T}$  is the scattering operator defined by:<sup>1,3</sup>

$$\mathbb{T} = [\mathbb{V}^{-1} - \mathbb{G}_0]^{-1} \tag{S5}$$

$\mathbb{T} = 0$  anywhere outside of the object  $n$ .

We begin our discussion with the definition of the absorption,  $P_{\text{abs}}$ , and scattering,  $P_{\text{sca}}$ , energy fluxes in terms of the  $\mathbb{T}$ -operator:<sup>4</sup>

$$P_{\text{abs}} = \frac{1}{2k_0 Z_0} \text{Tr} \left[ \left( \mathbf{E}^i \otimes \mathbf{E}^{i\dagger} \right) \mathbb{T}^\dagger \text{Asym} (-\mathbb{V}^{-1}) \mathbb{T} \right] \tag{S6a}$$

$$P_{\text{sca}} = \frac{1}{2k_0 Z_0} \text{Tr} \left[ \left( \mathbf{E}^i \otimes \mathbf{E}^{i\dagger} \right) \mathbb{T}^\dagger \text{Asym} (\mathbb{G}_0) \mathbb{T} \right] \tag{S6b}$$

which are derived from energy conservation and the relations:<sup>4</sup>

$$\mathbf{J}^s = \frac{i}{k_0 Z_0} \mathbb{V} \mathbf{E}^t \quad \text{and} \quad \mathbf{E}^s = \mathbb{G}_0 \mathbb{T} \mathbf{E}^i \tag{S7}$$

The absorption and scattering cross sections [Main text, Eqs. (1a) and (1b), respectively] are given respectively by,<sup>5</sup>

$$C_{\text{abs}} = P_{\text{abs}} / \frac{|E_0|^2}{2Z_0}, \quad C_{\text{sca}} = P_{\text{sca}} / \frac{|E_0|^2}{2Z_0}.$$

As discussed in the main text, to compute  $\langle C_{\text{abs}} \rangle$  and  $\langle C_{\text{sca}} \rangle$ , we need an expression for  $\langle \mathbf{E}^i \otimes \mathbf{E}^{i\dagger} \rangle$ . For an incident field of the form  $\mathbf{E}^i = E_0 e^{ik_0 \hat{\mathbf{k}}^i \cdot (\mathbf{r} - \mathbf{r}_0)}$ , where  $\hat{\mathbf{k}}^i$  is the direction of the plane wave and  $\mathbf{r}_0$  represent the origin of the field away from the object, and considering the two orthogonal polarization  $\hat{\mathbf{s}}$  and  $\hat{\mathbf{p}}$ :

$$\begin{aligned}
\langle \mathbf{E}^i \otimes \mathbf{E}^{i\dagger} \rangle &= \frac{1}{4\pi} \int_{4\pi} d\Omega |E_0|^2 [\hat{\mathbf{s}}\hat{\mathbf{s}} + \hat{\mathbf{p}}\hat{\mathbf{p}}] e^{ik_0 \hat{\mathbf{k}}^i \cdot (\mathbf{r} - \mathbf{r}')} \\
&= |E_0|^2 \frac{1}{4\pi} \int_{4\pi} d\Omega [\hat{\mathbf{s}}\hat{\mathbf{s}} + \hat{\mathbf{p}}\hat{\mathbf{p}}] \frac{1}{2} \left[ e^{ik_0 \hat{\mathbf{k}}^i \cdot (\mathbf{r} - \mathbf{r}')} + e^{-ik_0 \hat{\mathbf{k}}^i \cdot (\mathbf{r} - \mathbf{r}')} \right] \\
&= |E_0|^2 \frac{1}{4\pi} \int_{4\pi} d\Omega [\hat{\mathbf{s}}\hat{\mathbf{s}} + \hat{\mathbf{p}}\hat{\mathbf{p}}] \frac{1}{k_0^2} \int_0^\infty k_r^2 dk_r \frac{1}{2} [\delta(k_r - k_0) + \delta(k_r + k_0)] e^{ik_r \hat{\mathbf{k}}^i \cdot (\mathbf{r} - \mathbf{r}')} \\
&= |E_0|^2 \frac{2\pi}{k_0} \frac{1}{(2\pi)^3} \int_{-\infty}^\infty d^3 \mathbf{k} [\hat{\mathbf{s}}\hat{\mathbf{s}} + \hat{\mathbf{p}}\hat{\mathbf{p}}] \text{Im} \left( \frac{1}{k^2 - k_0^2} \right) e^{i\mathbf{k} \cdot (\mathbf{r} - \mathbf{r}')} \\
&= |E_0|^2 \frac{2\pi}{k_0} \text{Asym} \left( \frac{1}{(2\pi)^3} \int_{-\infty}^\infty d^3 \mathbf{k} [\mathbb{I} - \hat{\mathbf{k}}\hat{\mathbf{k}}] \frac{e^{i\mathbf{k} \cdot (\mathbf{r} - \mathbf{r}')}}{k^2 - k_0^2} \right) \\
&= |E_0|^2 \frac{2\pi}{k_0} \text{Asym}(\mathbb{G}_0), \tag{S8}
\end{aligned}$$

where the second step exploits the reciprocity of  $e^{ik_0 \hat{\mathbf{k}}^i \cdot (\mathbf{r} - \mathbf{r}')}$ , and the fourth step considers the identity<sup>6</sup>

$$\frac{1}{2} [\delta(k_r - k_0) + \delta(k_r + k_0)] = \frac{k_0}{\pi} \text{Im} \left( \frac{1}{k^2 - k_0^2} \right).$$

The penultimate expression corresponds to the plane-wave representation of the Dyadic Green function.<sup>2</sup> Substitution of Eq. (S8) into Eqs. (1a) and (1b) (Main text), respectively, leads the relations Eqs. (4a) and (4b) in the main text.

The asymmetry parameter is given by the force from scattering fields,  $\mathbf{F}^s$ , through the relation:<sup>7</sup>

$$\mu_{\text{sca}} C_{\text{sca}} = \frac{\omega}{k_0 I_0} \hat{\mathbf{k}}^i \cdot \mathbf{F}^s \tag{S9}$$

The projection of the scattering force,  $\hat{\mathbf{k}}^i \cdot \mathbf{F}^s$ , expressed in terms of the induced currents is given by:<sup>1,8</sup>

$$\begin{aligned}
\hat{\mathbf{k}}^i \cdot \mathbf{F}^s &= \hat{\mathbf{k}}^i \cdot \frac{1}{2\omega} \text{Im} \langle \mathbf{J}^s, \nabla \mathbf{E}^s \rangle \\
&= -\frac{1}{2\omega k_0 Z_0} \sum_j \text{Tr} \left[ \hat{\mathbf{k}}_j^i \left( \mathbf{E}^i \otimes \mathbf{E}^{i\dagger} \right) \mathbb{T}^\dagger \text{Sym}(\partial_j \mathbb{G}_0) \mathbb{T} \right], \tag{S10}
\end{aligned}$$

where we apply the relations from Eq. (S7).

Eq. (S10) represents a generalized form of the asymmetry parameter, regardless of the form of the source fields. Similarly to Eqs. (S6a) and (S6b), computation of the orientation average of,  $\hat{\mathbf{k}}^i \cdot \mathbf{F}^s$ , requires a direct expression for,  $\langle \hat{\mathbf{k}}_j^i \left( \mathbf{E}^i \otimes \mathbf{E}^{i\dagger} \right) \rangle$ :

$$\begin{aligned}
\langle \hat{\mathbf{k}}_j^i \left( \mathbf{E}^i \otimes \mathbf{E}^{i\dagger} \right) \rangle &= \frac{1}{4\pi} \int_{4\pi} d\Omega \hat{\mathbf{k}}_j^i (\hat{\mathbf{s}}\hat{\mathbf{s}} + \hat{\mathbf{p}}\hat{\mathbf{p}}) |E_0|^2 e^{ik_0 \hat{\mathbf{k}}^i \cdot (\mathbf{r} - \mathbf{r}')} \\
&= |E_0|^2 \frac{2\pi}{ik_0^2} \partial_j \text{Asym}(\mathbb{G}_0) \\
&= |E_0|^2 \frac{2\pi}{ik_0^2} \frac{\partial_j \mathbb{G}_0(\mathbf{r}, \mathbf{r}') - \partial_j \mathbb{G}_0^\dagger(\mathbf{r}', \mathbf{r})}{2i} \\
&= |E_0|^2 \frac{2\pi}{ik_0^2} \frac{\partial_j \mathbb{G}_0(\mathbf{r}, \mathbf{r}') + \partial_j \mathbb{G}_0^\dagger(\mathbf{r}', \mathbf{r})}{2i} \\
&= -|E_0|^2 \frac{2\pi}{k_0^2} \text{Sym}(\partial_j \mathbb{G}_0), \tag{S11}
\end{aligned}$$

where, in the third step, we consider the identity  $\partial'_j \mathbb{G}_0^\dagger(\mathbf{r}', \mathbf{r}) = -\partial_j \mathbb{G}_0^\dagger(\mathbf{r}', \mathbf{r})$ .<sup>9</sup> Substitution of Eqs. (S11) and (S10) into Eq. (S9), together with the relation  $\langle \mu_{\text{sca}} \rangle = \frac{\langle \mu_{\text{sca}} C_{\text{abs}} \rangle}{\langle C_{\text{sca}} \rangle}$  leads to the expression Eq. (4c) in the main text.

The expression Eqs. (4a), (4b) and (4c) in the main text, can be extended for linear, homogeneous and non-absorbing external medium, by replacing  $k_0$ , for  $n_0 k_0$ , where  $n_0$  is the refractive index of the external medium.

## S1.2 Surface-current BEM formulation

Particularly for the BEM, under the surface-current formulation, the fields and currents on an object  $n$  are, respectively, represented by the bi-linear expressions<sup>10,11</sup>

$$\phi_n = \begin{Bmatrix} \mathbf{E} \\ \mathbf{H} \end{Bmatrix} \quad \text{and} \quad \xi_n = \begin{Bmatrix} \mathbf{K} \\ \mathbf{N} \end{Bmatrix},$$

where  $\mathbf{K}$  and  $\mathbf{N}$  are the surface electric and magnetic current, respectively.

Using bi-linear expressions, the electromagnetic field is given by  $\phi_n = \mathbb{F}_n \xi_n$ . In this formula,

$$\mathbb{F}_n = ik_n \begin{bmatrix} Z_n \mathbb{G}_n & \mathbb{C}_n \\ -\mathbb{C}_n & \frac{1}{Z_n} \mathbb{G}_n \end{bmatrix}, \quad (\text{S12})$$

where  $\mathbb{C}_n = \frac{i}{k_n} \nabla \times \mathbb{G}_n$ , and  $k_n$  and  $Z_n$  are the wavevector and impedance of medium  $n$ , respectively.

Eq. (S15) in its bi-linear form is now expressed as:

$$\left[ \mathbb{H}_0 - ik_0 \mathbf{Z}_0^{-1} \mathbb{I} - \sum_n \mathbb{V}_n \right] \phi^t = 0,$$

where  $\mathbb{H}_0 = \begin{bmatrix} 0 & \nabla \times \\ -\nabla \times & 0 \end{bmatrix}$ ,  $\mathbf{Z}_0^{-1} = \begin{bmatrix} Z_0^{-1} & 0 \\ 0 & Z_0 \end{bmatrix}$ , and  $\mathbb{V}_n = ik_0 \mathbf{Z}_0^{-1} \begin{bmatrix} \epsilon_n - 1 & 0 \\ 0 & \mu_n - 1 \end{bmatrix}$ . Notice that in this case, the elements of  $\mathbf{V}$  and  $\mathbf{G}^0$ , are respectively given by  $\mathbb{V}_{nm} = \delta_{nm} \mathbb{F}_n^{-1}$ , and  $G_{nm}^0 = \mathbb{F}_0(\mathbf{r}_n, \mathbf{r}_m)$

The solution is obtained by expanding the surface currents on a particular basis,  $\mathbf{f}_r^n(\mathbf{r})$ , as:  $\xi_n(\mathbf{r}) = \sum_r x_r^n \mathbf{f}_r^n(\mathbf{r})$ , where the expansion elements  $x_r^n$  are obtained from boundary conditions. Further details can be found elsewhere.<sup>10,11</sup>

From the surface current expansion, the operators-based form of Eqs. (S18a), (S18b) and (S18c) is now given in matrix notations by:

$$\langle C_{\text{abs}} \rangle = \frac{2\pi}{k_0^2} \text{Tr} [\text{Sym}(G^0) W^\dagger \text{Sym}(-G^{\text{in}}) W] \quad (\text{S13a})$$

$$\langle C_{\text{sca}} \rangle = \frac{2\pi}{k_0^2} \text{Tr} [\text{Sym}(G^0) W^\dagger \text{Sym}(G^0) W] \quad (\text{S13b})$$

$$\langle \mu_{\text{sca}} C_{\text{sca}} \rangle = \frac{2\pi}{k_0^4} \sum_l \text{Tr} [\text{Asym}(\partial_l G^0) W^\dagger \text{Asym}(\partial_l G^0) W], \quad (\text{S13c})$$

where the elements of the  $G^0$  and  $G^{\text{in}}$  are respectively given by  $G_{ij}^{0, nm} = \langle \mathbf{f}_i^n, \mathbb{F}_0 \mathbf{f}_j^m \rangle$  and  $G_{ij}^{\text{in}, nm} = \delta_{nm} \langle \mathbf{f}_i^n, \mathbb{F}_m \mathbf{f}_j^m \rangle$ , and  $W = [G^{\text{in}} - G^0]$ . In this notation, the operator  $\langle \cdot, \cdot \rangle$ , denotes the conjugated inner product:  $\langle \mathbf{u}, \mathbf{v} \rangle = \int d^3r \mathbf{u}^\dagger(\mathbf{r}) \cdot \mathbf{v}(\mathbf{r})$ , where  $\mathbf{u}$  and  $\mathbf{v}$  are vector fields.

Note that due to the imaginary prefactor in Eq. (S12), the operators "Sym()" and "Asym()" in Eqs. (S13a), (S13b) and (S13c) are in opposite order in comparison with Eqs. (S18a), (S18b) and (S18c).

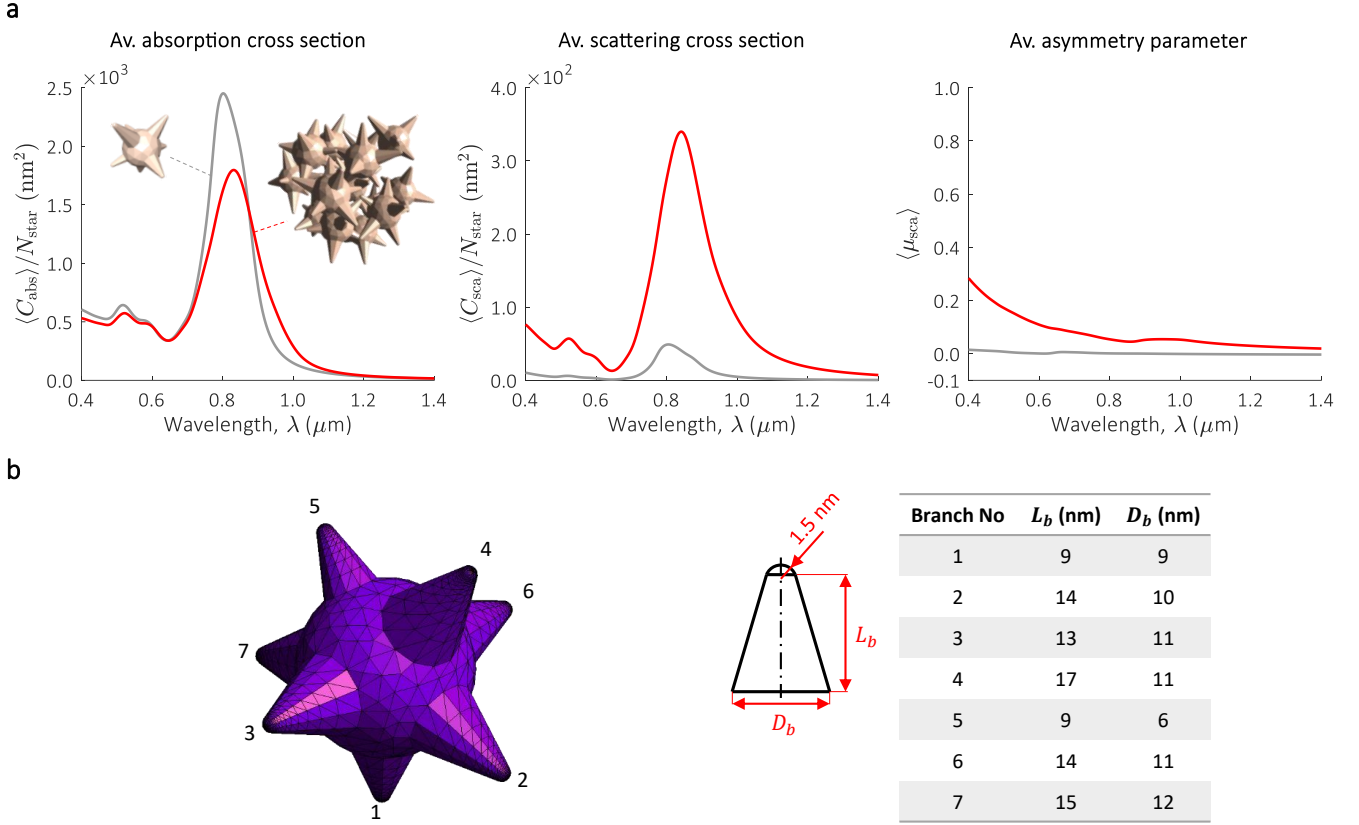


**Figure S1: Average light scattering of agglomerated gold nanostars** (a)  $\langle C_{\text{abs}} \rangle$ ,  $\langle C_{\text{sca}} \rangle$  and  $\langle \mu_{\text{sca}} \rangle$  of a single gold nanostar (grey) and cluster of agglomerated gold nanostars (red). The curves  $\langle C_{\text{abs}} \rangle$  and  $\langle C_{\text{sca}} \rangle$  are normalized to the number of stars ( $N_{\text{star}}$ ) for direct comparison. The cluster is based on 15 stars at 20% volume fraction. (b) Model of the star considered for the simulations. The model consist on a star with 7 legs with the dimensions indicated by the table at the right-hand side of the figure. All the simulations were performed by the BEM code for average light scattering simulations.<sup>12</sup> The refractive index of gold can be found elsewhere.<sup>13</sup>

Eqs. (S13a), (S13b) and (S13c) were implemented into a BEM application for average light scattering simulations.<sup>12</sup> The flexibility of the BEM algorithm enables to study objects of arbitrary morphology.<sup>10</sup> As a demonstration, we simulated the average light scattering parameters  $\langle C_{\text{abs}} \rangle$ ,  $\langle C_{\text{sca}} \rangle$  and  $\langle \mu_{\text{sca}} \rangle$  of a single gold nanostar and a cluster of agglomerated gold nanostars (Fig. S1). Fig. S1(a) illustrates the effects of interparticle coupling and interference of the scattered fields from the stars in cluster, which results in a reduction of  $\langle C_{\text{abs}} \rangle / N_{\text{star}}$  and an enhancement of  $\langle C_{\text{sca}} \rangle / N_{\text{star}}$  in comparison with a single star. Similarly, the scattering anisotropy is also clearly affected in the star cluster, as indicated by the variations in  $\langle \mu_{\text{sca}} \rangle$ . Fig. S1(b) shows the dimensions of the gold nanostar model considered for the simulations.

### S1.3 Efficiency of the theory against brute-force averaging methods.

Consider, for example, the computation of  $\langle C_{\text{sca}} \rangle$  by averaging over many plane-wave simulations at different angles of incidence (brute-force averaging). In terms of the Lippmann-Schwinger approach to scattering, this is equivalent to:

$$\langle C_{\text{sca}} \rangle = \frac{1}{k_0 |E_0|^2} \frac{1}{M} \sum_m^M \text{Tr} \left[ \left( \mathbf{E}_m^i \otimes \mathbf{E}_m^{i \dagger} \right) \mathbf{T}^\dagger \text{Asym} (\mathbb{G}_0) \mathbf{T} \right] \quad (\text{S14})$$

where  $m$  indicates a plane-wave simulations at a particular angle of incidence and polarization, and  $M$  is the total number simulations. This expression is constructed from the definition of  $C_{\text{sca}}$  for an incident field  $\mathbf{E}^i$  [Main text, Eq. (1b)].

Similar to other formulas derived in this work, Eq. (S14) is a general recipe that illustrates how to compute  $\langle C_{\text{sca}} \rangle$  using brute-force averaging. From this formula, we can deduct the steps required by any method of electromagnetic scattering, i.e.:

1. Determine the mathematical form of  $\mathbb{T}$  and  $\mathbb{G}_0$ , for a particular expansion basis.
2. Compute the expansion of  $\mathbf{E}_m^i$  using the particular basis.
3. Repeat "step 2"  $M$  times.
4. Replace  $\mathbf{E}_m^i$ ,  $\mathbb{T}$  and  $\mathbb{G}_0$  into Eq. (S14)

As discussed in the Section S1.6,  $M \geq 3$ , where  $M = 3$  correspond to the particular case of subwavelength particles.

On the other hand, as illustrated by Eq. (4b) in the main text, the theory of average light scattering does not require  $\mathbf{E}_m^i$ . Consequently, the computation of  $\langle C_{\text{sca}} \rangle$  is reduced to only two steps:

1. Determine the mathematical form of  $\mathbb{T}$  and  $\mathbb{G}_0$ , for a particular expansion basis.
2. Replacing  $\mathbb{T}$  and  $\mathbb{G}_0$  into Eq. (4b) of the Main text.

The same arguments apply for  $\langle C_{\text{abs}} \rangle$  and  $\langle \mu_{\text{sca}} \rangle$ . Thus, the theory of average light scattering enables more efficient computation of  $\langle C_{\text{abs}} \rangle$ ,  $\langle C_{\text{sca}} \rangle$  and  $\langle \mu_{\text{sca}} \rangle$ , than brute-force averaging methods.

## S1.4 Formulation for multiple objects

In the case of multiple objects Eq. (S1), becomes:

$$\left[ \mathbb{H}_0 - k_0^2 \mathbb{I} - \sum_{n=1}^N \mathbb{V}_n \right] \mathbf{E}^t = 0, \quad (\text{S15})$$

where  $N$  is the total number of objects. The solution of this equation is given by:<sup>1</sup>  $\mathbf{E}^t = \mathbf{E}^i + \sum_n \mathbb{G}_0 \mathbb{T}_n \mathbf{E}_n^i$ , and in matrix form:

$$\phi^t = \phi^i + \mathbf{G}^0 \mathbf{W} \phi^i \quad (\text{S16})$$

where  $\phi^i$  is a column vector, whose elements contain the incident fields on each object,  $\phi_n^i = \mathbf{E}_n^i$ ;  $\mathbf{W}^{-1} = \mathbf{G}_0 - \mathbf{V}^{-1}$  is the analogous of  $\mathbb{T}$  for a cluster;  $\mathbf{V}$  is a band matrix operator whose elements are  $\mathbb{V}_{nm} = \mathbb{V}_m \delta_{nm}$ ; and the matrix operator  $\mathbf{G}^0$  represents the interaction between the objects in the free space, whose elements are  $\mathbb{G}_{nm}^0 = \mathbb{G}_0(\omega; \mathbf{r}_n, \mathbf{r}_m)$ . The rest of the elements are defined in the main text.

Following the matrix notation, we extend the relations from Eq. (S7) to a vector form in terms of the induced current,  $\boldsymbol{\xi}^s$ , and fields,  $\phi^s$ :

$$\boldsymbol{\xi}^s = -\frac{i}{k_0 Z_0} \mathbf{V} \phi^t \quad \text{and} \quad \phi^s = \mathbf{G}^0 \mathbf{W} \phi^i. \quad (\text{S17})$$

Analogous to the derivation of  $\langle C_{\text{abs}} \rangle$ ,  $\langle C_{\text{sca}} \rangle$  and  $\langle \mu_{\text{sca}} \rangle$  for a single object, we use Eq. (S16) and the relations in Eq. (S17), to derive:

$$\langle C_{\text{abs}} \rangle = \frac{2\pi}{k_0^2} \text{Tr} \left[ \mathbf{W} \text{Asym}(\mathbf{G}^0) \mathbf{W}^\dagger \text{Asym}(-\mathbf{V}^{-1}) \right], \quad (\text{S18a})$$

$$\langle C_{\text{sca}} \rangle = \frac{2\pi}{k_0^2} \text{Tr} \left[ \mathbf{W} \text{Asym}(\mathbf{G}^0) \mathbf{W}^\dagger \text{Asym}(\mathbf{G}^0) \right], \quad (\text{S18b})$$

$$\langle \mu_{\text{sca}} \rangle = \frac{1}{\langle C_{\text{sca}} \rangle} \frac{2\pi}{k_0^4} \sum_j \text{Tr} \left[ \mathbf{W} \text{Sym}(\partial_j \mathbf{G}^0) \mathbf{W}^\dagger \text{Sym}(\partial_j \mathbf{G}^0) \right], \quad (\text{S18c})$$

these expressions represent the most general form of the average light scattering theory. They can be applied to single and group of particles, including heterogeneous collections of particles.

## S1.5 Formulation for an individual objects in a cluster

Using Eqs. (S18a), (S18b) and (S18c), we deduce the individual contribution of an object  $n$  in the cluster:

$$\langle C_{\text{abs}}^n \rangle = \frac{2\pi}{k_0^2} \text{Tr} [\mathbf{S}_{nn} \text{Asym} (-\mathbf{V}_n^{-1})] \quad (\text{S19a})$$

$$\langle C_{\text{sca}}^n \rangle = \frac{2\pi}{k_0^2} \left\{ \text{Tr} [\mathbf{S}_{nn} \text{Asym} (\mathbb{G}_{nn}^0)] + \sum_{n \neq m}^N \text{Tr} [\mathbf{S}_{nm} \text{Asym} (\mathbb{G}_{nm}^0)] \right\} \quad (\text{S19b})$$

$$\langle \mu_{\text{sca}}^n \rangle = \frac{N}{\langle C_{\text{sca}} \rangle} \frac{2\pi}{k_0^4} \sum_j \left\{ \text{Tr} [\mathbf{S}_{j,nn}^{\nabla} \text{Sym} (\partial_j \mathbb{G}_{nn}^0)] + \sum_{n \neq m}^N \text{Tr} [\mathbf{S}_{j,nm}^{\nabla} \text{Sym} (\partial_j \mathbb{G}_{nm}^0)] \right\}, \quad (\text{S19c})$$

where  $\mathbf{S} = [\mathbf{W} \text{Asym} (\mathbf{G}^0) \mathbf{W}^\dagger]$ , and  $\mathbf{S}_j^{\nabla} = [\mathbf{W} \text{Sym} (\partial_j \mathbf{G}^0) \mathbf{W}^\dagger]$ .

In Eqs. (S19b) and (S19c) the first and second term inside the curly brackets represent, self and interference scattering, respectively.<sup>14</sup> Note that  $\langle \mu_{\text{sca}}^n \rangle$  in Eq. (S19c) is scaled by  $N$  for better comparison with  $\langle \mu_{\text{sca}} \rangle$  from an isolated object.

To recover the total values of the cluster (Eqs. (S18a), (S18b) and (S18c)):

$$\begin{aligned} \langle C_{\text{abs}} \rangle &= \sum_{n=1}^N \langle C_{\text{abs}}^n \rangle \\ \langle C_{\text{sca}} \rangle &= \sum_{n=1}^N \langle C_{\text{sca}}^n \rangle \\ \langle \mu_{\text{sca}} \rangle &= \frac{1}{N} \sum_{n=1}^N \langle \mu_{\text{sca}}^n \rangle. \end{aligned}$$

## S1.6 Approximation for subwavelength particles

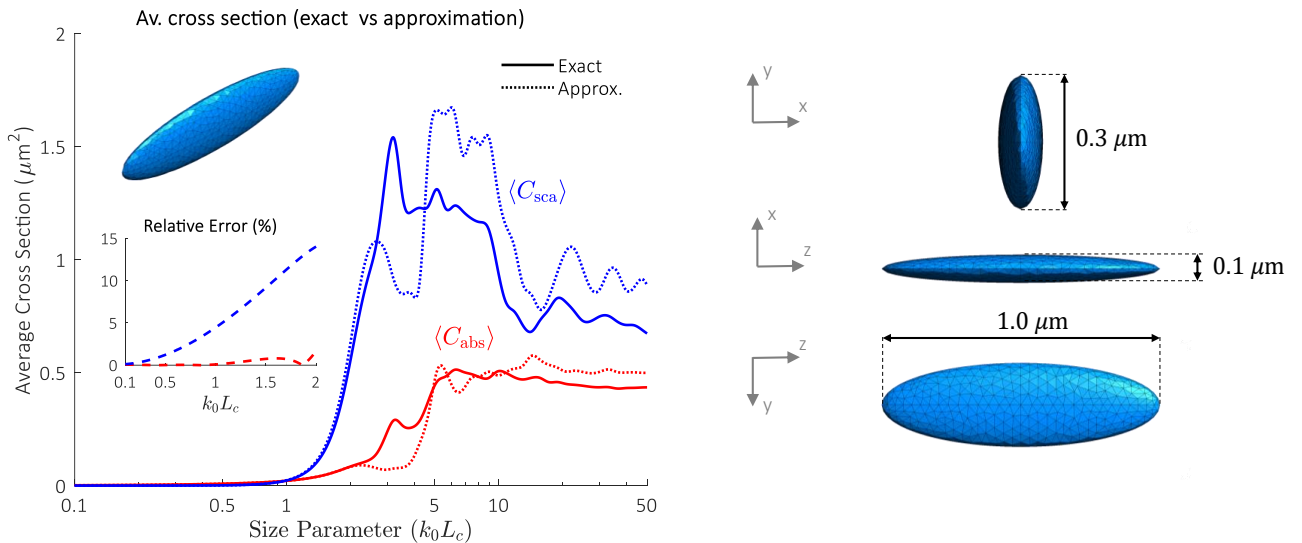


**Figure S2: Average light scattering of randomly oriented particles of subwavelength size. Comparison of exact solution and approximations** The figure shows  $\langle C_{\text{abs}} \rangle$  and  $\langle C_{\text{sca}} \rangle$  of a randomly oriented ellipsoid plotted against the size parameter  $k_0 L_c$  ( $L_c = 1.0 \mu\text{m}$ ). The exact solution for  $\langle C_{\text{abs}} \rangle$  and  $\langle C_{\text{sca}} \rangle$  is based on Eqs. (4a) and (4b) (Main text), respectively, and was computed by our BEM application for average light scattering simulations.<sup>12</sup> The approximated results are based on the relations,  $\langle C_{\text{abs}} \rangle \approx \frac{1}{3} (C_{\text{abs},x} + C_{\text{abs},y} + C_{\text{abs},z})$  and  $\langle C_{\text{sca}} \rangle \approx \frac{1}{3} (C_{\text{sca},x} + C_{\text{sca},y} + C_{\text{sca},z})$ . The inset shows the relative error between the approximated and the exact solutions for small size parameters. The dimensions of the ellipsoid are indicated at the right figure. The refractive index of the ellipsoid is  $N = 3.5 + 0.1i$ .

For small objects,  $\text{Asym}(\mathbb{G}_0) \approx \frac{k_0}{6\pi} \mathbb{I}$ ,<sup>15</sup> and,  $\mathbb{T} \approx 4\pi k_0 \boldsymbol{\alpha}$ ,<sup>a</sup> where  $\boldsymbol{\alpha}$  is the polarizability tensor. Substitution into Eq. (S19a), together with the relation

$$\mathbb{T}^\dagger \text{Asym}(-\mathbb{V}^{-1}) \mathbb{T} = \text{Asym}(\mathbb{T}) - \mathbb{T}^\dagger \text{Asym}(\mathbb{G}_0) \mathbb{T},$$

gives:

$$\langle C_{\text{abs}} \rangle = \frac{4\pi}{3} k_0 \text{Tr}[\text{Im}(\boldsymbol{\alpha})] - \frac{8\pi}{9} k_0^4 \text{Tr}|\boldsymbol{\alpha}|^2. \quad (\text{S20})$$

Because the particles are small, the second term in Eq. (S20) is negligible in comparison with the first, leading to Eq. (5) in the main text.

The second term in Eq. (S20) corresponds to the scattering of the particle, i.e.:

$$\langle C_{\text{sca}} \rangle = \frac{8\pi}{9} k_0^4 \text{Tr}|\boldsymbol{\alpha}|^2.$$

From this formula we deduct that the commonly used relation,<sup>17,18</sup>

$$\langle C_{\text{sca}} \rangle \approx \frac{1}{3} (C_{\text{sca},x} + C_{\text{sca},y} + C_{\text{sca},z}),$$

is valid only if  $\boldsymbol{\alpha}$  is a diagonal tensor. This is because,  $\text{Tr}|\boldsymbol{\alpha}|^2 \neq |\alpha_{xx}|^2 + |\alpha_{yy}|^2 + |\alpha_{zz}|^2$ , if  $\boldsymbol{\alpha}$  is a non-diagonal tensor.

In Fig. S2, we compute  $\langle C_{\text{abs}} \rangle$  and  $\langle C_{\text{sca}} \rangle$  for a randomly oriented ellipsoid, using the exact solution [Main text, Eqs. (4a) and (4b), respectively] and the approximation for small objects. The ellipsoid represents a typical case where  $\boldsymbol{\alpha}$  is not diagonal. As shown in the inset of Fig. S2, the approximation  $\langle C_{\text{sca}} \rangle \approx \frac{1}{3} (C_{\text{sca},x} + C_{\text{sca},y} + C_{\text{sca},z})$ , induces considerable error, even when  $k_0 L_c$  is small. On the other hand, the approximation for  $\langle C_{\text{abs}} \rangle$  [Main text, Eq. (5)], shows a small relative error ( $< 2\%$ ) for small particles ( $k_0 L_c < 2$ ). For larger particles ( $k_0 L_c > 2$ ), both approximations fail.

## S2 Average light scattering from fluctuational electrodynamics

### S2.1 Vacuum friction and averaged light scattering

An isolated object moving at a small velocity  $\mathbf{v}$  experiences a non-conservative friction force,  $\mathbf{F}_f$ , that results from the interaction with thermal fluctuations in the free space. To a first order approximation, the vacuum friction is given by,  $\mathbf{F}_f = -\hat{\gamma} \cdot \mathbf{v}$ , where  $\hat{\gamma}$  is the friction tensor given by:<sup>19</sup>

$$\hat{\gamma}_{ij} = \frac{2\hbar^2}{\pi k_B T} \int_0^\infty d\omega \frac{e^{\hbar\omega/k_B T}}{(e^{\hbar\omega/k_B T} - 1)^2} \text{Im}\{\text{Tr}[\partial_i (1 + \mathbb{G}_0 \mathbb{T}) \partial_j \text{Asym}(\mathbb{G}_0) \mathbb{T}^\dagger]\}, \quad (\text{S21})$$

here,  $k_B$  is the Boltzmann constant, and  $T$  is the equilibrium temperature of the system. Integrating the vacuum friction force over all solid angles leads to the relation,<sup>20</sup>  $\langle \mathbf{F}_f \rangle = \gamma \mathbf{v}$ , where  $\gamma = \sum_i \hat{\gamma}_{ii}$  is the friction coefficient.

From the relations,  $\partial_i \text{Asym}(\mathbb{G}_0) = -i \text{Sym}(\partial_i \mathbb{G}_0)$ ,<sup>19</sup> and,  $\partial_i^2 \text{Asym}(\mathbb{G}_0) = -k_0^2 \text{Asym}(\mathbb{G}_0)$ ,<sup>b</sup> the friction coefficient is expressed as:

$$\begin{aligned} \gamma = \frac{2\hbar^2}{\pi k_B T} \int_0^\infty d\omega \frac{e^{\hbar\omega/k_B T}}{(e^{\hbar\omega/k_B T} - 1)^2} \{ & k_0^2 \text{Tr}[\text{Asym}(\mathbb{G}_0) \text{Asym}(\mathbb{T})] \\ & - \sum_i \text{Tr}[\text{Sym}(\partial_i \mathbb{G}_0) \mathbb{T}^\dagger \text{Sym}(\partial_i \mathbb{G}_0) \mathbb{T}]\}. \end{aligned} \quad (\text{S22})$$

Applying Eqs. (4a) and (4b) (Main text) into the first term inside the curly brackets,<sup>c</sup> and Eq. (4c) (Main text) into the second, we derive Eq. (7) from the main text.

<sup>a</sup>the expression is deducted from the electric field generated by a point dipole<sup>16</sup>

<sup>b</sup>This expression is based on the fact that  $\text{Asym}(\mathbb{G}_0)$  can be expressed by propagating waves, as demonstrated in Eq. (S8)

<sup>c</sup>we consider the relation:  $\text{Asym}(\mathbb{T}) = -\mathbb{T}^\dagger \text{Asym}(\mathbb{T}^{-1}) \mathbb{T} = \mathbb{T}^\dagger \text{Asym}(\mathbb{G}_0 - \mathbb{V}^{-1}) \mathbb{T}$

## S3 Validation of average light scattering theory against analytical solutions

### S3.1 Average light scattering of randomly oriented spheroids

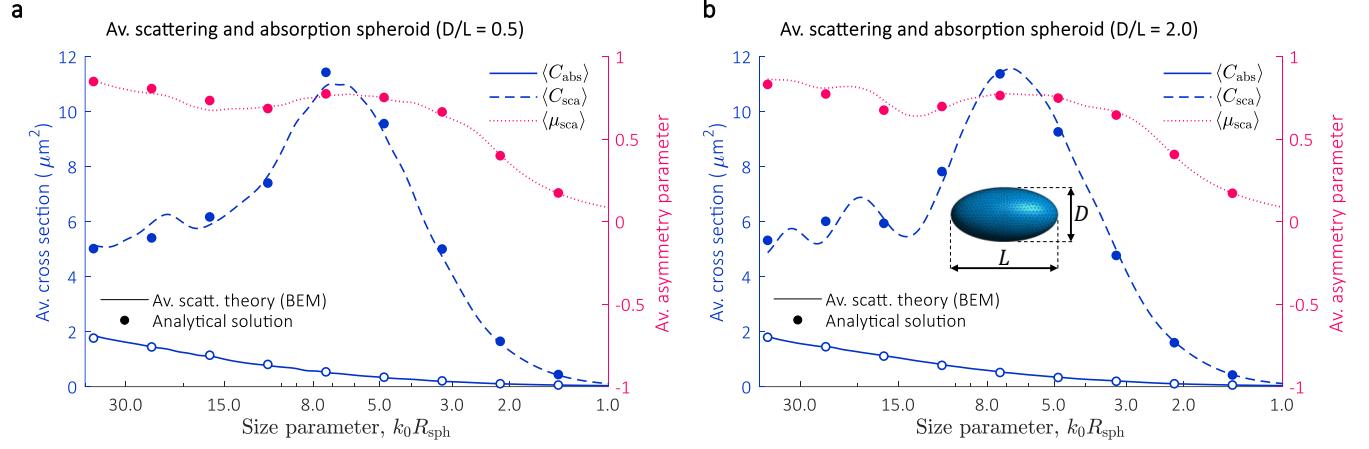


**Figure S3: Average light scattering of randomly oriented spheroids.**  $\langle C_{\text{abs}} \rangle$ ,  $\langle C_{\text{sca}} \rangle$  and  $\langle \mu_{\text{sca}} \rangle$  of (a) prolate ( $D/L = 0.5$ ) and (b) oblate spheroids ( $D/L = 2.0$ ), as a function of the size parameter  $k_0 R_{\text{sph}}$ , where  $R_{\text{sph}} = 1$  is the radius of a sphere with equivalent surface area.<sup>21</sup> The results are computed by the BEM code for average light scattering simulations,<sup>12</sup> and compared with the analytical solutions.<sup>22</sup> The dielectric constant of the ellipsoids is  $\epsilon_p = 2.2499 + 0.0240i$ . The principal and secondary axis of the prolate(oblate) spheroid are  $L = 1.5304(0.6016)$  and  $D = 0.7653(1.2032)$ , respectively.

We validate our code for average scattering simulations<sup>12</sup> against the analytical solution for prolate [Fig. S3(a)] and oblate [Fig. S3(b)] spheroids.<sup>22</sup> In terms of relative error, the agreement of the simulations for the prolate(oblate) spheroid is 3.6%(1.6%), 4.5%(3.7%) and 2.6%(3.2%) for  $\langle C_{\text{abs}} \rangle$ ,  $\langle C_{\text{sca}} \rangle$  and  $\langle \mu_{\text{sca}} \rangle$ , respectively. The discrepancy becomes more significant at short wavelengths, specifically at  $L_{\text{max}}/\lambda > 2.37(L_{\text{max}}/\lambda > 2.80)$  for the prolate(oblate) spheroid.

## S4 Validation of radiative transfer simulation against experiments

### S4.1 Characterization of as-grown $\text{VO}_2(\text{M})$ microcrystals

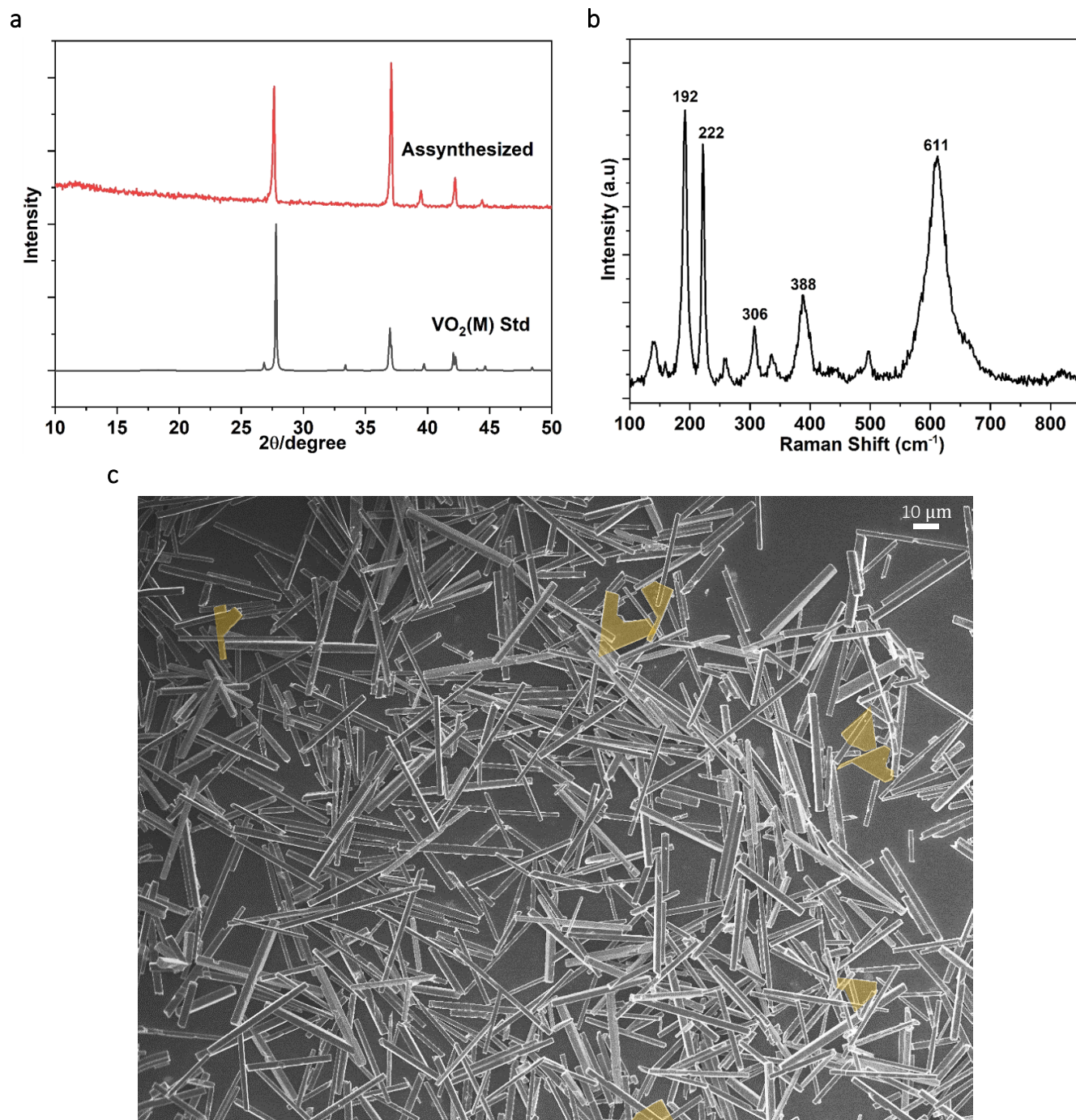


**Figure S4: Characterization of as-grown  $\text{VO}_2(\text{M})$  powder.** (a) X-ray diffraction and (b) Raman shift spectroscopy of  $\text{VO}_2(\text{M})$  microcrystals grown by hydrothermal synthesis (see Main Text, Materials and Methods). (c) SEM image of  $\text{VO}_2(\text{M})$  powder used for the estimation of size distribution [Main text, Fig. 3(c)]. Most crystals have a bar morphology with few having a larger flat morphology (flakes), which are marked in yellow.

## S4.2 Average light scattering of VO<sub>2</sub>(M) bars as a function of $L$ .

The sensitivity of the VO<sub>2</sub>(M) bars average light scattering to changes in  $L$  for  $W = 2.5 \mu\text{m}$  is shown in Fig. S5. As shown in the figure,  $\langle C_{\text{abs}} \rangle$ ,  $\langle C_{\text{sca}} \rangle$  and  $\langle \mu_{\text{sca}} \rangle$  show small variation at  $L > 15 \mu\text{m}$ . We noted a similar response for other values of  $W$  (not shown here).

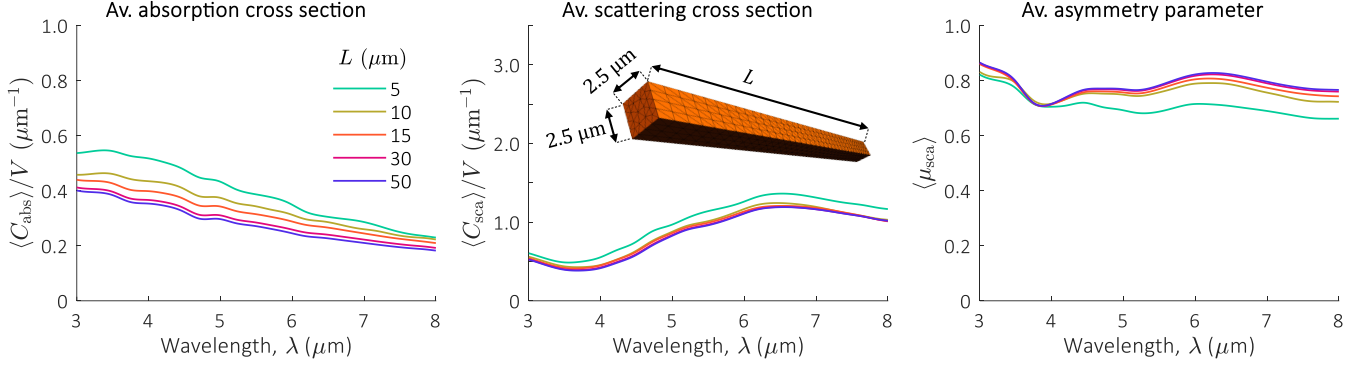


**Figure S5:**  $\langle C_{\text{abs}} \rangle$ ,  $\langle C_{\text{sca}} \rangle$  and  $\langle \mu_{\text{sca}} \rangle$  of VO<sub>2</sub>(M) bars of variable length and fixed width. The bars dimensions are:  $W = 2.5 \mu\text{m}$  and  $L = 5, 10, 15, 30$  and  $50 \mu\text{m}$ . The refractive index of the host,  $n_{\text{host}} = 1.5$ , and the refractive index of the VO<sub>2</sub>(M) bars was obtained from the literature (see "film 2" in Wan et al<sup>23</sup>).

## S4.3 Estimation of average light scattering of VO<sub>2</sub>(M) microcrystal ensemble

The average light scattering of the VO<sub>2</sub>(M) microcrystal ensemble is calculated through:

$$\langle C_{\text{abs}} \rangle = \sum_{W,L} F_{W,L} \langle C_{\text{abs}} \rangle_{W,L} + F_{\text{flake}} \langle C_{\text{abs}} \rangle_{\text{flake}} \quad (\text{S23a})$$

$$\langle C_{\text{sca}} \rangle = \sum_{W,L} F_{W,L} \langle C_{\text{sca}} \rangle_{W,L} + F_{\text{flake}} \langle C_{\text{sca}} \rangle_{\text{flake}} \quad (\text{S23b})$$

$$\langle \mu_{\text{sca}} \rangle = \frac{1}{\langle C_{\text{sca}} \rangle} \left[ \sum_{W,L} F_{W,L} \langle C_{\text{sca}} \rangle_{W,L} \langle \mu_{\text{sca}} \rangle_{W,L} + F_{\text{flake}} \langle C_{\text{sca}} \rangle_{\text{flake}} \langle \mu_{\text{sca}} \rangle_{\text{flake}} \right] \quad (\text{S23c})$$

where  $F$  represent the number microcrystals of a particular morphology in the ensemble, and the subscripts "W, L" and "flake", indicate a microbars of dimensions  $L$  and  $W$ , and flakes, respectively. For  $F_{W,L}$ , we considered the estimated size distribution (Main text, Fig. 3c), while  $F_{\text{flake}} = 5$ , as an approximate of the number of flakes found in the sample.

The volume of the microcrystal ensemble  $V$  is given by:

$$V = \sum_{W,L} F_{W,L} V_{W,L} + 5V_{\text{flake}}, \quad (\text{S24})$$

where  $V_{W,L}$  is the volume of a single bar with dimensions  $W$  and  $L$ , and  $V_{\text{flake}}$  is the volume of the flake structure.

## S4.4 Prediction of refractive index and scattering from PE films

Overall, the optical properties of PE are highly dependent on the crystallinity and the manufacturing process.<sup>24</sup> Thus, we extracted the complex refractive index of a pure PE film (101  $\mu\text{m}$  thick),  $n_{\text{PE}}$ , fabricated under the same conditions than those used for the composite films. First [Fig. S6(a)],  $T_{\text{tot}}$ ,  $T_{\text{spec}}$  and  $R_{\text{tot}}$  of the PE film were measured by FTIR and a gold integrating sphere (Main text, Materials and Methods). The real part of  $n_{\text{PE}}$  was obtained from Palik et al.<sup>24</sup> The extinction coefficient,  $\kappa_{\text{PE}} = \text{Im}(n_{\text{PE}})$ , was extracted from the equation:<sup>25</sup>

$$T_{\text{tot}} = \frac{(1 - R_f)^2 \exp(-2k_0 t_{\text{film}} \kappa_{\text{PE}})}{1 - R_f^2 \exp(-4k_0 t_{\text{film}} \kappa_{\text{PE}})},$$

where  $t_{\text{film}}$  is the thickness of the PE film and  $R_f$  is the reflectance at the air/PE interface.  $R_f$  was estimated from Fresnel law and the refractive index of PE from Palik et al.<sup>24</sup>

As shown in Fig. S6a,  $T_{\text{tot}} \neq T_{\text{spec}}$  at most parts of the spectrum, indicating a small scattering component in the film. To include this features in the modeling, we assume a small concentration of scattering particles inside the film. Because  $\kappa_{\text{PE}} \ll \text{Re}(n_{\text{PE}})$ ,  $T_{\text{tot}} \approx (1 - R_f)^2 \exp(-2k_0 t_{\text{film}} \kappa_{\text{PE}})$ .<sup>24</sup> Additionally, at low particle concentrations,<sup>26</sup>

$$T_{\text{spec}} \approx (1 - R_f)^2 \exp[(-f_v C_{\text{sca}}/V_p - 2k_0 \kappa_{\text{PE}}) t_{\text{film}}].$$

Thus, the scattering properties of the particles are extracted from:

$$C_{\text{sca}} = -\frac{V_p \ln(T_{\text{spec}}/T_{\text{tot}})}{f_v t_{\text{film}}}.$$

The extracted values of  $C_{\text{sca}}$  for  $f_v = 0.1\%$  v/v and particles of  $1 \mu\text{m}$  diameter are shown at the inset of Fig. S6(b). We fitted the results with a curve of the form  $C_{\text{sca}} = a/\lambda^b$ , with  $a = 2.4782$  and  $b = 1.4095$  [Fig. S6(b)]. Finally, using Monte-Carlo simulations (see Main Text, Materials and Methods) we iterate to find the value of  $\mu_{\text{sca}}$  that best matches the results of experiments. We found excellent agreement for  $\mu_{\text{sca}} = 0.75$  [Fig. S6(a)].

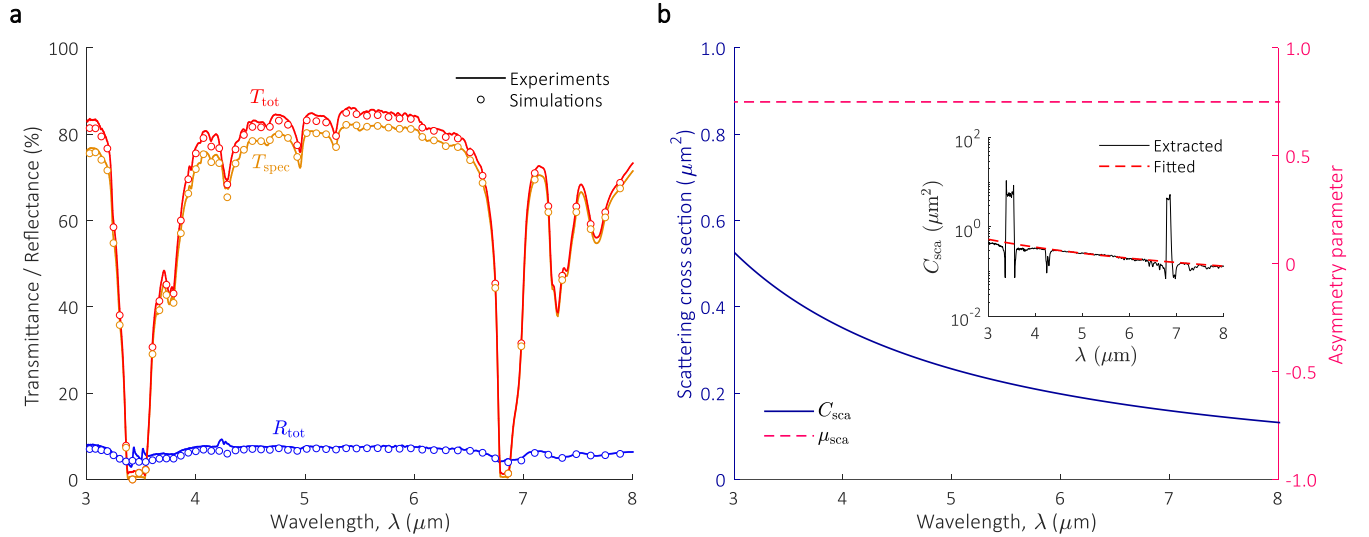


**Figure S6: Estimation of scattering properties and refractive index of the PE films used in the VO<sub>2</sub>(M)/PE composites.** (a) The values of  $T_{\text{tot}}$ ,  $T_{\text{spec}}$  and  $R_{\text{tot}}$  of a  $101\mu\text{m}$  thick PE film obtained from experiments (solid lines) are compared with Monte-Carlo simulations based on the estimated refractive index and scattering properties of the PE film). (b) Estimated  $C_{\text{sca}}$  of the PE film for  $f_v = 0.1\%$  v/v and particles of  $1 \mu\text{m}$  diameter. The curve is based on a fitting curve using the extracted results from experiments (inset).

## S4.5 Radiative properties of VO<sub>2</sub>(M)/PE composite films (Experiments and Simulations)

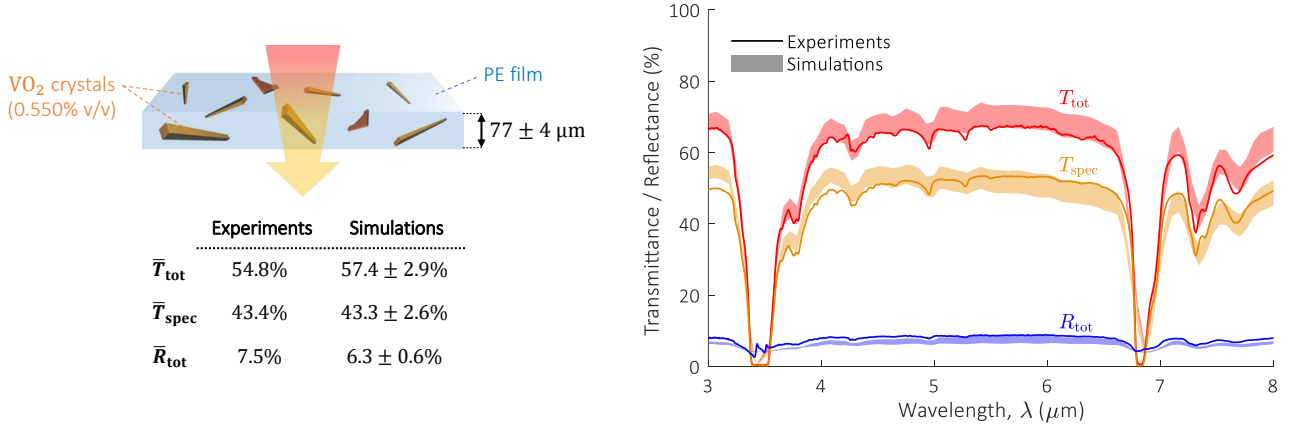


**Figure S7:**  $T_{\text{tot}}$ ,  $T_{\text{spec}}$  and  $R_{\text{tot}}$  of VO<sub>2</sub>(M)/PE composite film obtained from simulation and experiments. The composite film is composed of a PE matrix with 0.55% v/v VO<sub>2</sub>(M) powder and has  $77 \pm 4 \mu\text{m}$  thickness. The scattering properties of the VO<sub>2</sub>(M) powder are the same used in the main text [Fig. 4(a)]

## S5 Validation of Monte-Carlo Code

We validated our Monte-Carlo code for radiative transfer simulations against the Adding-doubling method [Fig. S8(b)]. We calculated the total transmittance ( $T_{\text{tot}}$ ) and reflectance ( $R_{\text{tot}}$ ), and the specular transmittance ( $T_{\text{spec}}$ ) at normal incidence over a 1 mm thick film with refractive index  $n_{\text{film}} = 1.4$ , and 0.1% particles per volume. The particles have a diameter  $D_p = 1 \mu\text{m}$ , and the scattering properties shown in Fig. S8(a).

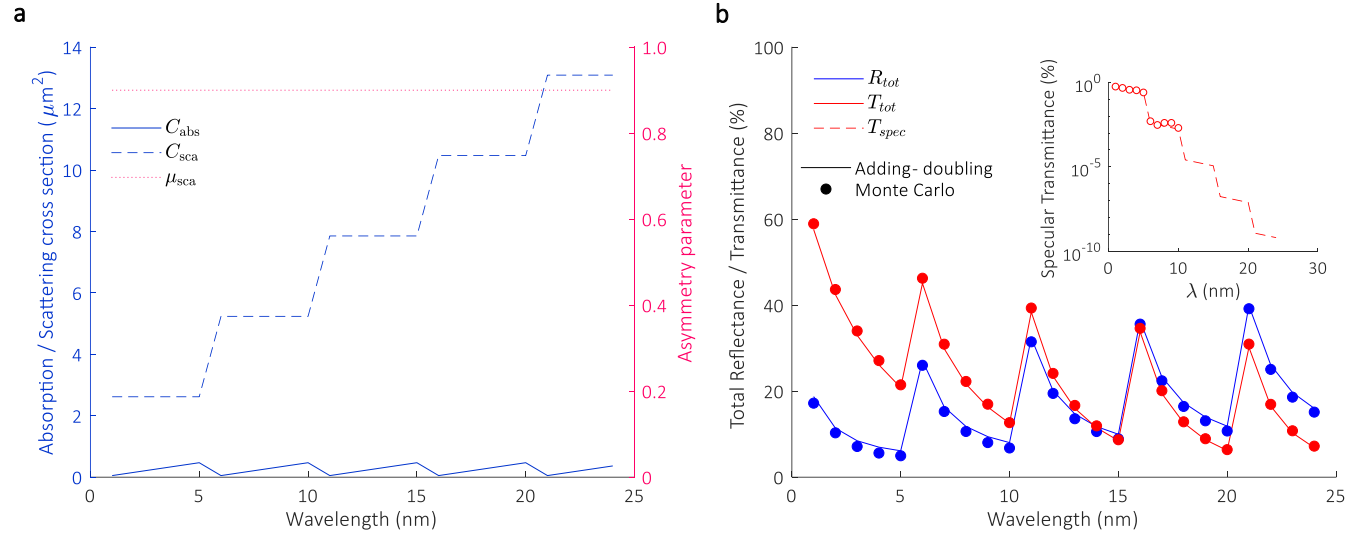


**Figure S8:** Validation of Monte-Carlo code for radiative transfer calculations against Adding-doubling method. (a) Light scattering properties  $C_{\text{abs}}$ ,  $C_{\text{sca}}$  and  $\mu_{\text{sca}}$  of the spherical particles ( $1 \mu\text{m}$  diameter) considered in this study (b) Total transmittance and reflectance and specular transmittance (inset) for light at normal incidence of a 1 mm thick film with 1.4 refractive index and 0.1% particles per volume. The results from our Monte-Carlo code (circles) are plotted against Adding-doubling method calculations using the code by Prahl.<sup>27</sup>

The results for Adding-doubling method are obtained from the open-source code by Prahl.<sup>27</sup> This code was used

to calculate the total reflectance and transmittance. The specular transmittance is calculated as

$$T_{\text{spec}} = (1 - R) \exp \left[ \frac{f_v}{V_p} (C_{\text{abs}} + C_{\text{sca}}) t_{\text{film}} \right],$$

where  $R = 4.12\%$  is the reflectance of a 1 mm thick film with 1.4 refractive index,  $f_v$  is the volume fraction,  $V_p$  is the particle’s volume, and  $t_{\text{film}}$  is the thickness of the film.

The results of total transmittance/reflectance from our Monte-Carlo code show excellent agreement with the curves from Adding-doubling method. The specular transmittance (inset of Fig. S8) shows good agreement up to 10 nm wavelength. Outside this range, the values of specular transmittance are below the minimum resolution of our Monte-Carlo setup (0.0001% for 1,000,000 photons).

We performed an additional test based on the total transmittance and reflectance of a slab with particles, considering the conditions:  $n_{\text{film}} = 1.0$ ,  $t_{\text{film}} = 200 \mu\text{m}$ ,  $D_p = 1 \mu\text{m}$ ,  $f_v = 0.1\%$ ,  $C_{\text{abs}} = 0.5236 \mu\text{m}^2$ ,  $C_{\text{sca}} = 4.7124 \mu\text{m}^2$  and  $\mu_{\text{sca}} = 0.75$ . The results shown in Table 1, show excellent agreement against the exact solution from Van de Hulst<sup>28</sup> and simulations with two different Monte-Carlo codes.<sup>29,30</sup>

$R_{\text{tot}}$	$T_{\text{tot}}$	Source
9.739%	66.096%	Van de Hulst <sup>28</sup>
9.774%	66.101%	Monte Carlo code
9.734%	66.096%	Wang, Jacques and Zheng <sup>29</sup>
9.711%	66.159%	Prahl et al <sup>30</sup>

**Table 1: Validation of Monte-Carlo code for Test 1.** Total transmittance and reflectance of a slab with particles, considering the conditions:  $n_{\text{film}} = 1.0$ ,  $t_{\text{film}} = 200 \mu\text{m}$ ,  $D_p = 1 \mu\text{m}$ ,  $f_v = 0.1\%$ ,  $C_{\text{abs}} = 0.5236 \mu\text{m}^2$ ,  $C_{\text{sca}} = 4.7124 \mu\text{m}^2$  and  $\mu_{\text{sca}} = 0.75$

## References

1. Krüger, M. *et al.* “Trace formulas for nonequilibrium Casimir interactions, heat radiation, and heat transfer for arbitrary objects”. *Physical Review B* **86**, 115423 (2012).
2. Tsang, L. *et al.* *Scattering of Electromagnetic Waves: Theories and Applications*, 445 (John Wiley & Sons, Inc., New York, USA, 2000).
3. Molesky, S. *et al.* “T Operator Bounds on Angle-Integrated Absorption and Thermal Radiation for Arbitrary Objects”. *Physical Review Letters* **123**, 257401 (2019).
4. Molesky, S. *et al.* “Global T operator bounds on electromagnetic scattering: Upper bounds on far-field cross sections”. *Physical Review Research* **2**, 033172 (July 2020).
5. Bohren, C. F. & Huffman, D. R. *Absorption and Scattering of Light by Small Particles*, 544 (John Wiley & Sons, Inc., 1998).
6. Chew, W. C., Sha, W. E. & Dai, Q. I. “Green’s Dyadic, Spectral Function, Local Density of States, and Fluctuation Dissipation Theorem”. *Progress in Electromagnetics Research* **166**, 147–165 (2019).
7. Mishchenko, M. I. “Radiation force caused by scattering, absorption, and emission of light by nonspherical particles”. *Journal of Quantitative Spectroscopy and Radiative Transfer* **70**, 811–816 (2001).
8. Polymeridis, A. G. *et al.* “Fluctuating volume-current formulation of electromagnetic fluctuations in inhomogeneous media: Incandescence and luminescence in arbitrary geometries”. *Physical Review B* **92**, 134202 (Oct. 2015).
9. Tai, C.-T. *Dyadic Green Functions in Electromagnetic Theory* 2nd (ed Dudley, D. D.) 343 (IEEE Press Series, New York, USA, 1994).
10. Rodriguez, A. W., Reid, M. T. & Johnson, S. G. “Fluctuating-surface-current formulation of radiative heat transfer: Theory and applications”. *Physical Review B* **88**, 054305 (Aug. 2013).
11. Reid, M. T. & Johnson, S. G. “Efficient Computation of Power, Force, and Torque in BEM Scattering Calculations”. *IEEE Transactions on Antennas and Propagation* **63**, 3588–3598 (2015).

12. Ramirez-Cuevas, F. V. *AVESCATTER: A SCUFF-EM application for light scattering of randomly oriented particles of arbitrary shape*. 2020.
13. Ciesielski, A. *et al. Surface Science* **674**, 73–78 (Aug. 2018).
14. Mishchenko, M. I., Hovenier, J. W. & Travis, L. D. *Light scattering by nonspherical particles: theory, measurements, and applications* 1st, 720 (Academic Press, 2000).
15. Novotny, L. & Hecht, B. *Principles of Nano-Optics* 1st (Cambridge University Press, Cambridge, UK, 2006).
16. Jackson, J. D. *Classical Electrodynamics* 3th, 832 (John Wiley & Sons, New York, 1998).
17. Santiago, E. Y. *et al.* “Efficiency of Hot-Electron Generation in Plasmonic Nanocrystals with Complex Shapes: Surface-Induced Scattering, Hot Spots, and Interband Transitions”. *ACS Photonics* **7**, 2807–2824 (2020).
18. Muskens, O. L. *et al.* “Quantitative absorption spectroscopy of a single gold nanorod”. *Journal of Physical Chemistry C* **112**, 8917–8921 (2008).
19. Golyk, V. A., Krüger, M. & Kardar, M. “Linear response relations in fluctuational electrodynamics”. *Physical Review B* **88**, 155117 (2013).
20. Mkrtchian, V. *et al.* “Universal thermal radiation drag on neutral objects”. *Physical Review Letters* **91**, 220801 (2003).
21. Mishchenko, M. I., Travis, L. D. & Macke, A. “Scattering of light by polydisperse, randomly oriented, finite circular cylinders”. *Applied Optics* **35**, 4927–4940 (1996).
22. Mishchenko, M., Travis, L. & Mackowski, D. *T-Matrix Codes for Computing Electromagnetic Scattering by Nonspherical and Aggregated Particles*.
23. Wan, C. *et al.* “On the Optical Properties of Thin-Film Vanadium Dioxide from the Visible to the Far Infrared”. *Annalen der Physik* **531**, 1900188 (2019).
24. Palik, E. D. & Ghosh, G. *Handbook of optical constants of solids*, 999 (Academic Press, 1998).
25. Katsidis, C. C. & Siapkas, D. I. “General transfer-matrix method for optical multilayer systems with coherent, partially coherent, and incoherent interference”. *Applied Optics* **41**, 3978 (2002).
26. Prah, S. A., van Gemert, M. J. C. & Welch, A. J. “Determining the optical properties of turbid media by using the adding–doubling method”. *Applied Optics* **32**, 559–568 (1993).
27. Prah, S. A. *Forward and Inverse Radiative Transport using the Adding-Doubling method*. 2017.
28. Van de Hulst, H. C. *Multiple light scattering : tables, formulas, and applications* 1st, 332 (Academic Press, New York, USA, 1980).
29. Jacques, S. L. & Wang, L. “MCML—Monte Carlo modeling of light transport in multi-layered tissues”. *Computer Methods and Programs in Biomedicine* **47**, 131–146 (1995).
30. Prah, S. A. *A Monte Carlo model of light propagation in tissue*. in *SPIE Proceedings: Dosimetry of Laser Radiation in Medicine and Biology* **10305** (1989), 102–111.